Spring 2023

Optimizing the Placement of Multiple UAV--LiDAR Units Under Road Priority and Resolution Requirements

Zachary Michael Osterwisch
Missouri University of Science and Technology

Department:

OPTIMIZING THE PLACEMENT OF MULTIPLE UAV–LIDAR UNITS UNDER ROAD PRIORITY AND RESOLUTION REQUIREMENTS

by

ZACHARY MICHAEL OSTERWISCH

A THESIS

Presented to the Graduate Faculty of the

MISSOURI UNIVERSITY OF SCIENCE AND TECHNOLOGY

In Partial Fulfillment of the Requirements for the Degree

MASTER OF SCIENCE

in

COMPUTER ENGINEERING

2023

Approved by:

Dr. Ahmad Alsharoa, Advisor
Dr. Steven Corns
Dr. Joe Stanley

ABSTRACT

Real-time road traffic information is crucial for intelligent transportation systems (ITS) applications, like traffic navigation or emergency response management, but acquiring such data is tremendously challenging in practice because of the high costs and inefficient placement of sensors. Some modern ITS applications contribute to this problem by equipping vehicles with multiple light detection and ranging (LiDAR) sensors, which are expensive and gather data inefficiently; one solution that avoids vehicle-mounted LiDAR acquisition has been to install elevated LiDAR instruments along roadways, but this approach remains unrefined. The eventual development of sixth-generation (6G) wireless communication will enable new, creative solutions to solve these challenges. One new solution is to deploy multiple multirotor unmanned aerial vehicles (UAVs) outfitted with LiDAR sensors (ULiDs) to acquire data remotely. These ULiDs can capture accurate and real-time road traffic information for ITS applications while maximizing the capabilities of LiDAR sensors, which in turn reduces the number of sensors required. Accordingly, this thesis aims to find the optimal 3D placement of multiple ULiDs to maximize road coverage efficiency for ITS purposes. The formulated optimization problem is constrained by unique ULiD specifications, including field-of-view (FoV), point cloud resolution, geographic information system location, and road segment coverage priorities. A computational intelligent algorithm based on particle swarm optimization is proposed to solve the designed optimization problem. Furthermore, this thesis illustrates the benefits of using the proposed algorithm over existing baselines.

ACKNOWLEDGMENTS

I want to thank my advisor, Dr. Ahmad Alsharoa, for guiding me through both my undergraduate degree and my master's degree. He saw potential in me since day one and has helped me to leverage my skills to their fullest. I would also like to thank my committee members, Dr. Joe Stanley and Dr. Steven Corns, for their assistance in my endeavors: Dr. Stanley for his invaluable advice that helped me navigate my undergraduate program, and Dr. Corns for helping me recognize and develop my passion for computational intelligence of which I was entirely unaware. Lastly, I owe my family and friends a colossal debt of gratitude; I would not have made it this far without them.

TABLE OF CONTENTS

Page

LIST OF ILLUSTRATIONS

LIST OF TABLES

NOMENCLATURE

Symbol	Description
A^g	Area of segment g.
A^λ_{cov}	Coverage area for ULiD λ.
E_o	Penalizing constant.
G	Set of road segments.
H^λ	Half-length of the horizontal FoV coverage for ULiD λ.
I^g	Continuous, normalized importance factor of segment g.
M	Arbitrarily large value.
R^g_{min}	Minimum resolution requirement of segment g based on its importance I^g.
R^λ	Resolution provided by ULiD λ.
R_o	Maximum coefficient value for the minimum resolution requirement.
V^λ	Half-length of the vertical FoV coverage for ULiD λ.
Λ	Set of ULiDs.
$\mathbf{\Omega}$	Defined 3D problem space containing segments G and all possible placement positions for ULiDs Λ.
δ^g_x	x-coordinate distance from segment g to ULiD position x^λ.
δ^g_y	y-coordinate distance from segment g to ULiD position y^λ.
ϵ^λ	Binary value indicating whether ULiD λ is being utilized.
$\eta^{\lambda g}$	Binary value indicating whether segment g is covered by ULiD λ.
λ	ULiD.
μ^λ	Binary value indicating whether ULiD λ is rotated about the z axis.
ϕ	ULiD vertical FoV angle.
θ	ULiD horizontal FoV angle.
ξ_{min}	Minimum percentage of segments G that must be covered by ULiDs Λ.
a	Side length of a segment.
g	Road segment.

n^{λ}_{scan}	Scan rate of ULiD λ.
x^{λ}	Continuous x coordinate for ULiD λ.
x^{g}	Center x-coordinate of segment g.
y^{λ}	Continuous y coordinate for ULiD λ.
y^{g}	Center y-coordinate of segment g.
z^{λ}	Continuous z coordinate for ULiD λ.

1. INTRODUCTION

Since the 1960s, the phenomenon known as urbanization, the process by which populations migrate from rural to urban areas, has been accelerating around the globe [1]. The global population reached a remarkable milestone in 2007, as shown in Figure 1.1, with more than half of all people worldwide residing in urban areas, and projections suggest that 7 in 10 people will live in urban areas by the year 2050 [1, 2, 3]. This figure is even higher in the United States, whose urban areas are predicted to sustain 75% of the country's populace by the same year, according to the Department of Transportation [4]. Unfortunately, crowded urban areas are typified by highly complicated road networks, high pedestrian and vehicle densities, unpredictable behaviors, new constructions, and accidents, all of which frequently result in the blockage of roads and disturb the normal flow of traffic. It follows, then, that modern transportation infrastructures must drastically improve and scale with the densification of urban areas.

1.1. TRAFFIC CONGESTION

Upgrades to transportation infrastructure—specifically capacity—are made urgently necessary by the expansion of urban areas. This strain is particularly apparent in the United States, whose transportation infrastructure is already reaching its limit; according to the United States Census Bureau, 85% of its total workforce (totaling more than 130 million people) drove to work in 2019 [5, 6]. As urbanization progresses, the number of cars in urban areas grows, ultimately worsening the congestion due to traffic. A decades-long trend of increasing commute times to and from work in the United States is evident in Figure 1.2a, with the average one-way travel time for the 130 million drivers in 2019 approaching 28 minutes. Likewise, Figure 1.2b shows how travel times fewer than 10 minutes have decreased

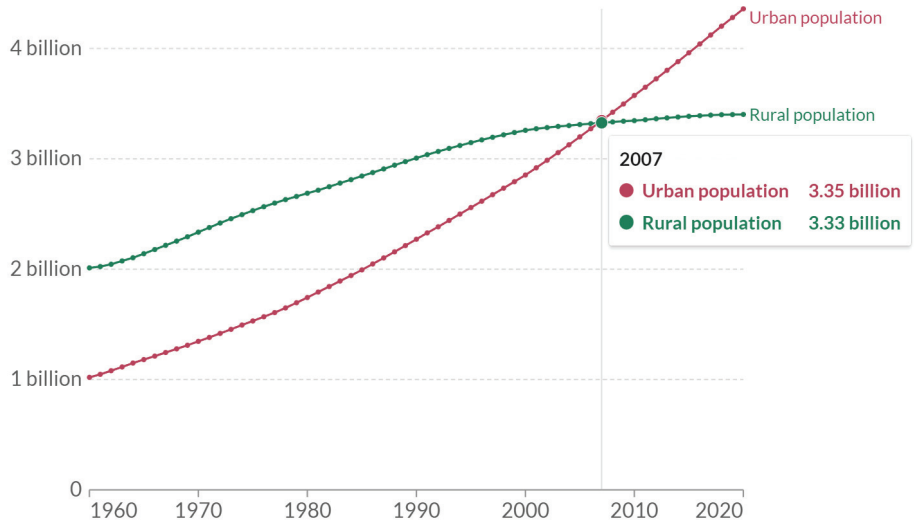

Figure 1.1. Time series of the numbers of people living in urban and rural areas worldwide [2].

while travel times exceeding 60 minutes have risen, contributing to the overall increase in the average travel time. These data clearly reflect how urbanization can increase the average commute time, increasing the demand for infrastructure improvements.

1.2. PUBLIC SAFETY

Such improvements and the provision of timely navigation data are similarly necessary for public safety. In addition to causing more drivers to be on the road for longer periods, an increased population density swells the demand for (and thus the congestion due to) freight, which plays a crucial role in the economy; specifically, United States' "freight system moves approximately 63 tons of goods per American each year," and this volume is expected to increase more than 40% by 2045 [4]. Moreover, rises in demand cause freight to become increasingly concentrated in large, expanding urban areas. Together with the increased average travel time, due to the rise in the number of urban commuters, and the heightened stress on the freight system, due to the increase in demand, two prominent effects on public safety emerged: vehicle accidents and environmental pollution.

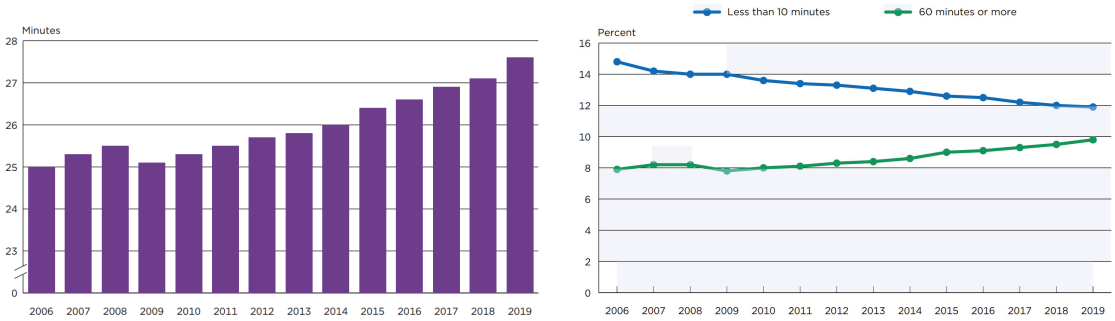

(a) Average travel time.

(b) Traveling fewer than 10 minutes or greater than/equal to 60 minutes.

Figure 1.2. Travel times to work in the United States from 2006 to 2019 [7]

1.2.1. Vehicular Accidents. Although design advances and technological breakthroughs have improved vehicle safety over the years, vehicle accident-related deaths have not diminished. The number of people killed each year on roadways reached approximately 1.35 million in 2018, and in the United States, vehicle accidents are the leading cause of death for people aged 1–54 years old [8]. From 2020 to 2021, the number of vehicle accident-attributable deaths increased by 10.5%, totaling almost 43,000 deaths; this number represents the highest traffic fatality rate in the United States since 2005. Furthermore, vehicle crash deaths increased 18% between 2019 and 2021, the most significant two-year increase since 1946 [9]. While these additional fatalities cannot be attributed solely to urbanization, more vehicles on urban roads nevertheless complicate existing congestion and make vehicle crash fatalities more likely to occur.

1.2.2. Environmental Pollution. The increase in the number of vehicles on urban streets also contributes to a rise in environmental pollution. Pollution has become a predominant global concern, particularly the rampant emission of greenhouse gases, which have been identified as the cause of anomalous warming trends worldwide [10, 11, 12]. These amplified temperatures have had profound impacts on the global population as a result of increased flooding, rising sea levels, stronger hurricanes, hazards to animal and plant

life, and more [11]. Although a variety of greenhouse gases (including methane, nitrous oxide, and fluorinated gases) play a role in these warming temperatures, the abovementioned detrimental effects are attributed primarily to carbon dioxide (CO_2), an alarming amount of which (75% of all greenhouse gas emissions worldwide) is emitted into the atmosphere, with transportation being the principal source in countries around the globe, including the United States [10, 13]. Unfortunately, studies have already shown that commute times rise as urbanization expands, as demonstrated in Figure 1.2, and longer periods of driving cause proportionally greater amounts of CO_2 to be ejected into the atmosphere. Figure 1.3a shows different projections of global carbon emissions for the 21st century based on projections from the Intergovernmental Panel on Climate Change (IPCC) given certain representative concentration pathways (RCP) scenarios, and Figure 1.3b displays the projected global temperature increases under the same RCP conditions. According to these predictions, even under a relatively low-emission scenario (i.e., without immediate and drastic reductions in carbon emissions), the global temperature will rise a minimum of 4°F by the end of the century. These data clarify the situation markedly: the sooner carbon emissions are reduced, the better the world will be. In the context of this research, improving transportation infrastructure with timely navigation data can help reduce the largest source of CO_2 emissions—transportation—by reducing driving times.

1.2.3. Issues with Emergency Response Management. Urbanization corresponds to an increased population density in urban areas, requiring first responders such as ambulances, firefighters, and police officers to service larger populations in smaller geographical areas. Furthermore, without improvements to the existing transportation infrastructure, rising populations in urban areas lead to anomalously long travel times and a high occurrence frequency of vehicle accidents. The consequence of this worsening traffic situation is more accidents to which emergency services must respond under increasingly oppressive conditions [14, 15, 16]. One journal article [14] looked at emergencies attributable to California wildfires over a 7-year period and examined the correlation between traffic and emergency

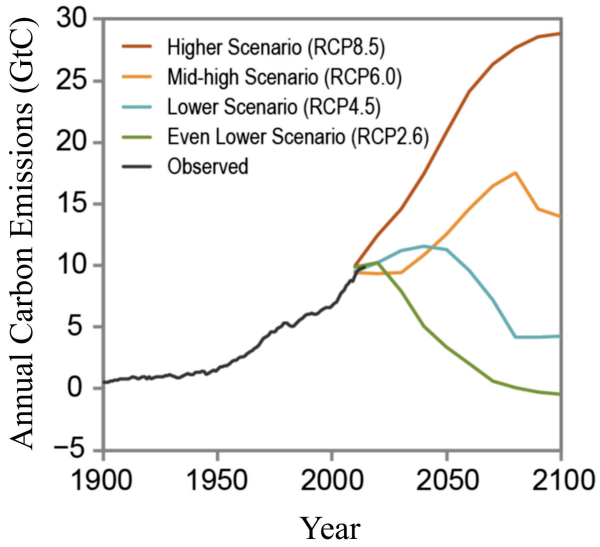

(a) Hypothetical RCP scenarios of carbon emissions in gigatonnes of carbon (GtC) based on global climate model predictions given different socioeconomic and emission inputs.

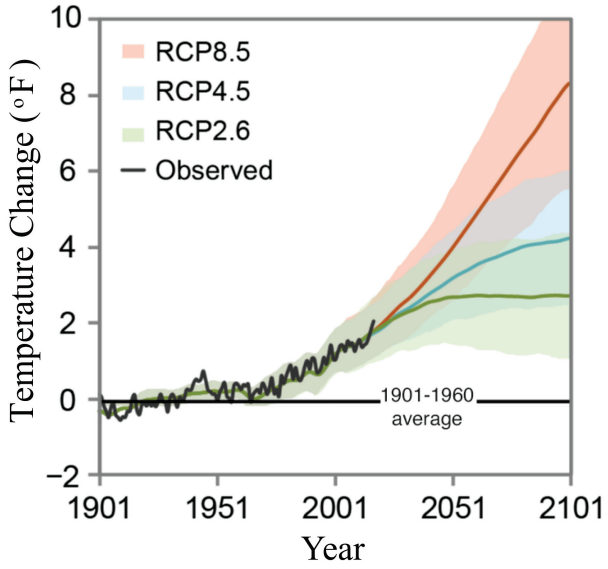

(b) Projected temperature increases relative to the 1901–1960 average based on different RCP scenarios.

Figure 1.3. Projected global carbon emissions and temperatures based on IPCC model predictions [12].

response times. The authors concluded that traffic was directly correlated to delays in the response times of fire trucks and medical personnel; the cascading effects of these delays further impacted other emergency endeavors. These findings are consistent with data published in 2022 [16] indicating that the response times for emergency and non-emergency calls in New Orleans doubled and tripled, respectively, between 2019 and 2022 and that, while other factors appeared to contribute to the rise in response times, traffic congestion was the leading cause. As such, providing timely traffic navigation data is crucial for traffic management, public safety, and emergency response [4, 14].

Emergency response services can also refer to the management of evacuation routes. In particular, it is critical to evacuate people to safety during both natural (e.g., wildfires and floods) and human-made (e.g., terrorist attacks) disasters, the frequencies and severities of which are increasing in the wake of climate change [17]. The United States Census Bureau estimated that 3.4 million adults, or 1.4% of the adult population, were evacuated from their homes in 2022 [18], although the trend of this statistic, which the Census Bureau first recorded in 2020 to monitor the increase in evacuations over the last decade, is not yet known [19]. Deploying a safe and effective evacuation system will remain essential as urbanization continues and evacuation routes become increasingly complex. Therefore, real-time services such as route navigation, accident avoidance, and accurate traffic network monitoring can reduce traffic congestion and enhance network flow.

1.3. TRANSPORTATION INFRASTRUCTURE SOLUTIONS

The demand for improved transportation infrastructure is not new; both local, state, and federal governmental entities and private companies have been working for decades to improve transportation infrastructure. Nevertheless, this demand is accelerating due to urbanization and population growth. Physical road improvements, such as adding lanes, paving new roads, and improving intersections, represent a traditional approach to meet this demand. However, physically altering road networks in urban areas is not always

Figure 1.4. Global intelligent transportation system market, 2020-2024 [27].

possible due to spatial limitations. More recently, the rise of digital technology in the 1970s and 1980s has yielded a new approach to implement such improvements: intelligent transportation systems (ITS) [20, 21, 22, 23]. ITS, which aims to improve safety and minimize congestion by assisting with traffic and mobility management [24, 25], combines information and communication technologies "to increase information to users of roadways and transit systems and make managing the assets and infrastructure more efficient and effective" [26]. As shown in Figure 1.4, the ITS industry is currently estimated to have a compound annual growth rate (CAGR) of almost 10%, with the largest growth projected in North America.

While ITS has become commonplace in modern society, the industry has taken decades to evolve. Early ITS technology was integrated into urban areas first by the public sector, i.e., by local governments and by state-run departments of transportation (DOTs) that build and operate urban roadways. One example of an early ITS technology is the traffic light, which emerged in the 1970s with the use of in-ground sensors to detect traffic [20, 28]. Dynamic message signs (DMSs) are another early application of ITS [20]; at present, DMSs are commonly placed alongside roadways to display various warnings, for instance, informing road users of traffic congestion, accidents, work zones, or changing speed limits. Over the years, new technologies such as cameras and radars were incorporated into ITS to

acquire data over larger tracts of space [22]. Among the most crucial implements of ITS, however, are traffic management centers (TMCs), which have been deployed throughout the public sector [20]. These TMCs were created as information hubs to collect and process data (e.g., weather, traffic speeds, and accidents) relevant to a road system. The decision to collect numerous types of data and then to process the data at a centralized location has been necessary for the continued success and progress of ITS [24]. Among these types of ITS data, timely spatial data about the transportation infrastructure are among the most impactful, as real-time geospatial data can inform TMCs about current road conditions (such as traffic conditions and accidents) and allow the system to make better-informed decisions.

Geographic information systems (GIS) was among the early technologies applied for ITS. In the United States, GIS functionality pivots around the Global Positioning System (GPS), and was first developed in the 1970s (and remains operated) by the military. Since the 1980s, however, GPS has been broadly utilized for vehicle navigation [29, 30]. Private companies utilized GPS to create digital maps for vehicles before the technology evolved into onboard GPS devices by the late 1990s. However, in those days, GPS functionality was limited and unreliable because the United States military distorted the GPS signals [30, 31]. The technology was also very costly for the general public, with a GPS navigation system costing hundreds of dollars to own; nevertheless, GPS has advanced by leaps and bounds since its conception. The military removed its restriction on GPS in the early 2000s, allowing the technology to yield more precise locations, and the cost of GPS has drastically diminished over time. With the help of modern technological advancements, GPS has become an integral part of everyday life for transportation needs in both the public and the private sectors. However, the private sector has undoubtedly benefited more from the technology, with many private applications (colloquially referred to as “apps”) utilizing GPS services built into most smartphones.

Today, millions of drivers in the United States utilize ITS via GPS navigation. Some studies estimate that more than 164 million people, or 68% of drivers, used apps on their smartphones to help them navigate in 2022, although some estimates reach as high as 93% of drivers [32, 33]. The most popular navigation app among drivers is Google Maps, which was downloaded more than 24 million times in 2022 and is favored by 67% of app users; the other 33% of app users appear to be evenly split between Apple Maps and Waze [34, 35]. These kinds of apps utilize GPS to help users reach their destination by providing possible routes and an estimated time of arrival (ETA) for each potential route. Most apps allow routes to be selected based on the shortest distance, shortest time, or fewest number of turns and can give users directions based on a manually selected mode of transportation, such as personal vehicle, train, bicycle, or bus.

1.4. ARTIFICIAL INTELLIGENCE APPLICATIONS IN ITS

The route-planning performance of navigation apps has recently been improved using new data sources and computer algorithms. In particular, technological advances have enabled a variety of tools to be used in conjunction with GPS to assist ITS. The most prominent example is artificial intelligence (AI), which enables computers to find patterns and learn from large data sets to improve their output; computers can typically learn these patterns far better and faster than humans with the help of AI. As a result, all of the leading apps (including the abovementioned Google Maps, Apple Maps, and Waze) use AI to improve their navigation and route-planning accuracy [35]. In the context of navigation, these AI algorithms are fed many types of data, such as GPS data, business hours, past traffic conditions, satellite images, weather conditions, and user-reported events or locations. Nevertheless, although these apps are continuously improving, and while these algorithms are capable of achieving more efficient route navigation with more accurate ETAs [36, 37], there remain many drawbacks to the app solution.

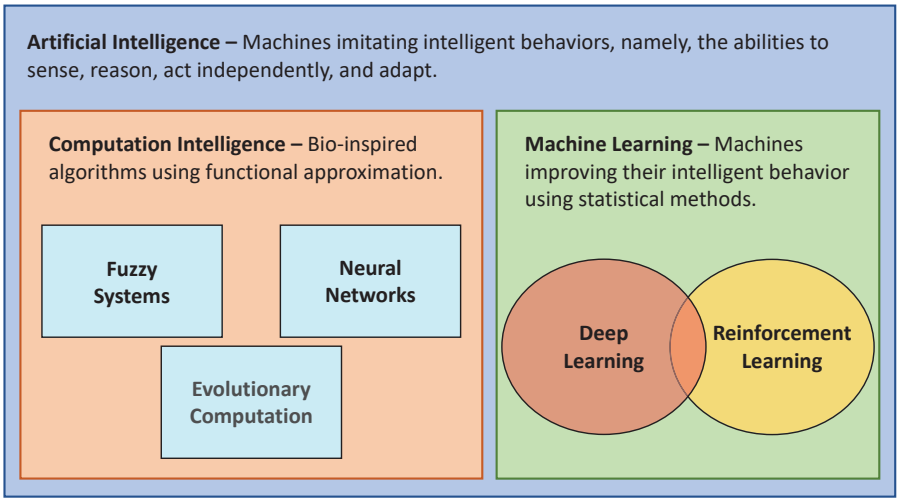

Figure 1.5. Schematic depicting AI and the relationships among its sub-fields.

The use of the term "AI" originated in 1955, when it was first coined by Stanford professor John McCarthy [38, 39, 40]. Since then, references to AI, defined as "the science and engineering of making intelligent machines, especially intelligent computer programs" [38], have become prevalent in today's society, with terms such as machine learning (ML), computational intelligence (CI), deep learning (DL), and reinforcement learning (RL) becoming commonplace. However, these terms are sometimes used interchangeably, which is incorrect; rather, although some of these sub-fields may overlap, each one exhibits its own distinct attributes. In fact, AI encompasses all of these sub-fields, as visualized by the interrelationship among AI, ML, CI, DL, and RL in Figure 1.5; consequently, "AI" has become an umbrella term. Nevertheless, AI is composed of two major sub-fields: ML and CI. ML focuses on using statistical methods to improve the behavior of a machine (e.g., a computer). An ML algorithm always requires a training phase in which the machine "learns" the data before it can output the desired results. RL and DL are sub-fields of ML and refer to specific algorithm training methods.

CI, sometimes called "soft computing", is the other major sub-field of AI and constitutes the focus of this thesis. CI is defined as "the theory, design, application, and development of biologically and linguistically motivated computational paradigms" [41, 42]. This definition essentially means that biological organisms inspire CI algorithms, and when such techniques are successfully designed and deployed, they allow computers to learn a specific task using data and/or experimental observations. These algorithms started to gain traction within the AI community in the 1980s [42]. Unlike ML methods, CI algorithms do not always need to be trained, so they can typically be deployed more easily than can ML approaches. CI comprises three main sub-fields that, while all being capable of being applied within the ML domain, are not necessarily ML techniques: neural networks, fuzzy systems, and evolutionary computation. This thesis utilizes the lattermost of the three CI sub-fields. Evolutionary computation is the idea that individuals in a population become "fitter" over time through biological processes, such as adaptation, natural selection, and selective breeding. A popular example of an evolutionary computation algorithm that adopts these concepts (specifically, the behaviors of populations searching for food and reproducing over generations) is particle swarm optimization (PSO).

PSO is a population-based, bio-inspired stochastic optimization algorithm that was created in 1995 by Kennedy and Eberhart, who hypothesized that groups of animals traveling as a collective entity (e.g., schools of fish or flocks of birds) maximize their rewards when the experiences gained by its individual members are shared amongst the group; moreover, shared experiences by the group can increase positive outcomes and minimize unfavorable results [43]. The application of PSO has increased dramatically over the last decade [44]; in fact, numerous previous studies [45, 46, 47, 48] have utilized PSO in similar ways to solve non-convex optimization problems. Particularly challenging (e.g,. high-dimensional) problems can be computationally expensive in terms of both the time and the computing resources necessary to perform an exhaustive global search for the solution. In this context, PSO algorithms can be quite useful: they typically demand fewer resources

and can yield near-optimal solutions at computational speeds exponentially greater than those of deterministic models. Furthermore, the optimization problem designed for this thesis contains discrete functions, so the problem is not differentiable; however, PSO does not require the problem to be differentiable, making it suitable for solving nonlinear problems [49].

Centralized processing, such as that performed within TMCs, is what enables ITS to thrive; however, each privately operated navigation app can access only the data it collects. In other words, public ITS applications do not have access to private companies' data and vice versa. This disconnect between systems means that the AI algorithms used in navigation apps are trained on incomplete urban data sets. Figure 1.6 provides one example of an AI-trained navigation app that is optimized to minimize travel times but is unaware of the entire scope of the urban area. The scenario in this figure is described as follows [50]:

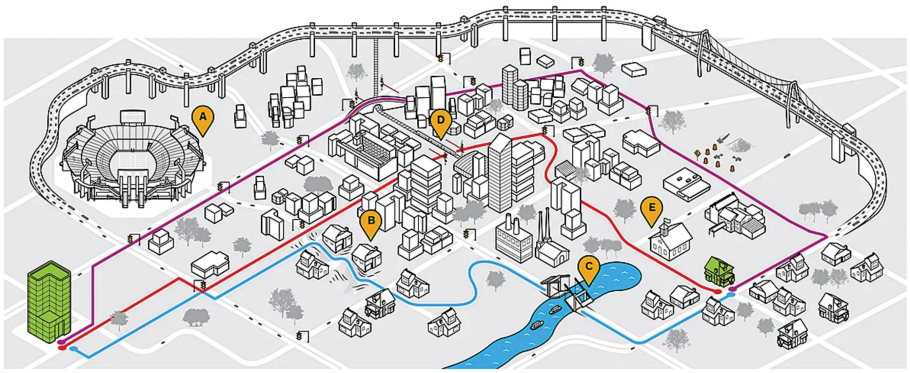

Figure 1.6. An example of routing inadequacy by smartphone navigation apps [50].

> A sporting event at a nearby stadium [A] causes a traffic backup on the highway that bypasses the center of this imaginary urban area. That's a problem for our hypothetical driver trying to get home from work, so she turns to a navigation app for help. The shortest—and, according to the app, the fastest—alternate route [blue line] winds through a residential neighborhood with blind turns,

> a steep hill [B], and a drawbridge [C], which can create unexpected delays for those unfamiliar with its scheduled openings. The red route cuts through the city center [D] and in front of an elementary school [E]; the app doesn't know school just let out for the day. Fortunately, our driver knows the area, so she selects the purple route, even though the app indicates that it isn't the fastest option. Drivers unfamiliar with the area and looking for a shortcut to the stadium could find themselves in chaotic—even hazardous—situations.

The above example aptly demonstrates how these apps ignorantly and ineffectively route their users. Such apps can utilize the vast wealth of private data, such as individuals' travel routes, speeds, and travel times, to improve their navigation guidance; however, the data provided by individual app users limit the apps' realm of knowledge by precluding a full understanding of the urban environment. Furthermore, forfeiting these data poses a risk to the user: such apps can track an individual on the road, and since these apps are tied to the individual's smartphone, these data can be wielded maliciously to the detriment of the user, thereby constituting an enormous security risk [51, 52]. On the other hand, public ITS applications in urban areas act within their own realm of incomplete information, including access to general information collected about the urban environment through public surveillance technologies such as radar, video cameras, and other sensors [22]; however, these systems lack the capability to gather or utilize real-time GPS data about individual drivers. Hence, ITS technologies are deficient in real-time spatial knowledge about the urban environment that, if collected, would greatly improve these systems' ability to more efficiently and effectively manage assets and infrastructure.

1.5. RELATED ITS RESEARCH

The ITS industry is growing and fueling the need for solutions to improve the system. Thus, the ability to capture greater amounts of real-time spatial data is an intense research focus. Light detection and ranging (LiDAR) sensors (colloquially termed 'LiDARs') are capable of providing such data to ITS and have been replacing the normal video camera. LiDARs project a multitude of laser beams across their field of view (FoV) and measure the time it takes for the beam to return, allowing the distance between the sensor aperture and the object(s) from which the laser beam has reflected to be calculated [53]. This process is repeated hundreds of thousands (sometimes millions) of times per second, and the resulting data is called a point cloud. Point cloud data consist of attributes such as 3D coordinates, time, and the intensity of the returned signal [54]. Current state-of-the-art LiDARs have an accuracy typically within a couple of centimeters [55, 56, 57]. Since these sensor measurements represent distances, the 3D point cloud data generated do not contain normal RGB values that video cameras provide, thus preserving personal identifiable information (PII); a comparison between the notable aspects of LiDARs and video cameras is shown in Table 1.1. Hence, highly accurate, privacy-conserving 3D data maps can be generated for an urban environment in real time when LiDAR data is coupled with a GPS. This is why LiDAR sensors are among the most critical for ITS applications [58, 59].

Table 1.1. LiDAR versus video camera characteristics.

	LiDAR Sensor	Video Camera
Data Output	3D point cloud	RGB data
3D Information	Provided	Not provided
Privacy	Does not reveal PII	Reveals PII
External Illumination	Not required	Required except for thermal cameras
Optical Illusions	Negligible	Subject to

Many authors who conduct ITS research have exploited the benefits of LiDAR to improve the quality of their work [59, 60, 61, 62, 63, 64, 65, 66, 67, 68, 69, 70, 71, 72]. Numerous scholars have focused on the ability of LiDAR to aid autonomous vehicles (AVs), which can subsequently provide ITS data. One review [60] covers the many uses and benefits of LiDAR in AVs, such as its powerful potential to perform object detection and tracking, which are capabilities necessary for numerous ITS applications (e.g., AV navigation). Likewise, some researchers [61] built upon the use of LiDAR for object tracking to propose a method that automatically annotates the lane markings on roadways to assist AV driving. The detection of objects assists in AV navigation, but when LiDAR is paired with GPS, it can also aid in vehicle localization [62, 63, 64].

However, equipping every AV with LiDAR imposes high computational and financial costs. For instance, to ensure their safety and reliability, AVs require multiple high-end LiDAR sensors to sense their surroundings at all angles and perspectives, with each LiDAR sensor costing tens of thousands of dollars; furthermore, these AVs then require a powerful graphics processing unit (GPU) to process the data efficiently in real time, and a GPU capable of processing LiDAR data costs thousands of dollars; finally, processing all the data required for autonomous driving consumes thousands of watts [65]. These effects dramatically raise the cost of AVs while reducing fuel efficiency by up to 10% [73]. In addition, although reducing the operational costs of LiDARs is crucial to their widespread use in ITS applications, LiDARs are limited by another consideration: they produce tremendous amounts of data. Capturing the millions of data points per second needed to construct accurate 3D maps results in the acquisition of several gigabytes per second [74]. As a result, many works have aimed to reduce the processing cost of LiDAR data [66, 67, 68], and their findings will be crucial in advancing the use of LiDAR in ITS applications; however, installing multiple LiDAR sensors on every AV still yields enormous amounts of data and comes at a steep financial cost.

An alternative to mounting multiple LiDAR sensors on every AV is to mount them along roadways [59, 69, 70, 71, 72]. Unlike sensors installed around the body of an AV, elevated LiDAR sensors (ELiDs) deployed at elevated positions along a roadway can perceive more of the surrounding urban environment and enjoy an unobstructed FoV. In addition, this approach would require far fewer LiDAR arrays for ITS applications, such as navigation and traffic management. Lucic et al. [69] were the first to investigate the optimal placement of ELiDs along a roadway while considering the energy and throughput constraints required to efficiently process the data in a backhaul network in real-time; they then expanded upon their research by optimizing the connected backhaul network that the ELiDs use to communicate data [70]. Other scholars [71] focused on the fifth-generation (5G) wireless communication between the backhaul infrastructure operating with ELiDs and the AVs on the road. [59] considered the real-time communication between a cloud-based server and an ELiD and between the ELiD and AVs. Even though ELiDs are not mounted on AVs, the sensors can still help with driving decisions, as shown by Ali et al. [72]. However, the ELiDs proposed in the stated works are placed only meters above the ground, for instance, on lampposts or streetlights. Consequently, this strategy would still necessitate hundreds of LiDAR sensors to cover an urban environment, and while the final number of ELiDs may be less than the number of AV-mounted LiDARs, ELiDs do not maximize the potential of LiDAR sensors insomuch that state-of-the-art LiDAR sensors can provide highly detailed and accurate maps at distances exceeding 100 meters [55, 56, 57]. Thus, it would be greatly valuable to utilize even fewer LiDAR sensors while still capturing relevant, highly precise data for ITS applications, thereby reducing costs and the overall volume of data.

Multirotor unmanned aerial vehicles (UAVs) have been around since the early 20th century, but only in the last two decades have the technology and price improved to the point where they can be routinely deployed for commercial and consumer use [75, 76, 77]. Many recent works have focused on the potential wireless communication capabilities that

UAVs can provide for ITS purposes. [78] proposed a UAV-direct protocol to assist with mobile device-to-device communication. Alsharoa et al. [79] similarly studied UAVs as relays for wireless communication with the aim of optimizing the placement of relay UAVs. [80] proposed a vehicular ad hoc network in which UAVs communicate with vehicles and other UAVs. Assi et al. [81] and Alsharoa et al. [82] proposed UAV path planning solutions in a dynamic environment to serve AVs and mobile communication needs, respectively. Unfortunately, the current capabilities of 5G wireless communication do not allow UAVs to provide the necessary information (e.g., LiDAR data) in real time. It is because of this limitation that UAVs in ITS are utilized mainly for communication needs instead of being deployed to gather information.

Nevertheless, communication technology continues to undergo dramatic developments, and UAVs are continually benefiting from this evolution. As a result, UAVs have recently been deployed for emerging communication technologies, such as intelligent reflecting surfaces (IRS) and the sixth generation of wireless communication (6G) [83, 84, 85, 86]. In cooperation with technologies such as IRS, 6G is projected to enable peak wireless transfer speeds of one terabyte per second [87], which is two orders of magnitude greater than the theoretical speed of 5G (only 10 gigabytes/second) [88, 89]. Accordingly, UAVs armed with 6G capabilities will transcend their current design objective as communication devices for ITS applications and achieve the ability to perform both information and communication applications. One future UAV application of interest is attaching LiDARs to UAVs for real-time ITS purposes.

For more than four decades, numerous industries have deployed UAVs equipped with LiDARs (ULiDs) for mapping purposes [90], although none were real-time applications. For example, Lucieer et al. [91] developed a ULiD for forest inventory applications, while Fowler et al. [92] and Wei and Jian [93] used ULiDs for topographic scanning and analyzing data, respectively, and Salvaggio and Sun in [94] detected and modeled buildings using data collected by ULiDs. As ITS has become increasingly relevant due to urbanization, research

has focused more on the benefits of utilizing LiDAR technology, but the unwieldy amounts of data produced by LiDARs have forced previous ITS studies to connect LiDARs directly to a backhaul network or to a GPU (in the case of AV-mounted LiDARs).

Nevertheless, while 5G cannot currently support the wireless real-time transfer needs of LiDAR applications, the emerging 6G technology will be more than capable, and thus, the real-time utilization of ULiDs is an emerging field of research. One previously discussed study [81] on the use of UAVs for communication in ITS focused on the communication between AVs and UAVs, and the authors suggested that LiDAR as a potential data source could be valuable in real-time ITS applications. Anand et al. [95] streamed LiDAR data in real-time with low latency over the internet; it should be noted, however, that their model considered only one LiDAR, and that sensor did not transmit from a UAV. Unfortunately, relatively few other works have focused on potential real-time ULiD applications that could be realized given the inevitable evolution of communication technology capable of providing the necessary transfer speeds. One such study [96] investigated a vehicle identification method and a vehicle speed measurement method based on ULiD data. Similarly, Chen et al.[97] proposed a real-time ULiD approach for the detection of power transmission lines. In this context, this thesis investigates a potential application of ULiDs in ITS, namely, the acquisition of real-time traffic navigation data by multiple ULiDs, and aims to find the optimal placement of those ULiDs within an urban environment.

1.6. THESIS SCOPE AND CONTRIBUTIONS

As evidenced above, LiDARs and the precise 3D maps they can produce in real-time are indispensable for ITS applications. LiDARs are currently the dominant type of sensor mounted onto AVs to collect data on driving in urban environments, and many researchers are studying how to exploit LiDAR technology to provide accurate ITS data about urban environments. However, because LiDARs are relatively expensive and generate large amounts of data, finding a way to utilize fewer sensors while still providing the same

or improved data quality is of considerable interest. As an alternative to outfitting AVs with numerous LiDAR sensors for the sake of collecting ITS data, LiDARs have been mounted at elevated positions (i.e., ELiDs) along urban roadways. This method utilizes fewer sensors, which in turn reduces their financial burden and diminishes the amount of ITS data that must be processed. However, ELiDs do not maximize the FoV potential of LiDAR sensors, and thus, many sensors are still needed to provide adequate coverage of urban roadways. Of course, some roadways may not always require coverage (e.g., during non-peak travel times), but because ELiDs are fixed, they cannot adapt to temporal variations in traffic. One alternative is to deploy ULiDs. Attaching LiDAR sensors to UAVs provides the sensor with an aerial view of the environment and thus maximizes their FoV potential. Moreover, ULiDs require fewer LiDAR sensors than do ELiDs to cover the same area, and since ULiDs are maneuverable, they have the ability to cover (or not cover) roadways as demanded by the ITS need for data.

In consideration of the above, this thesis considers multiple ULiDs that are being operated in an urban environment to capture LiDAR data from roadways of interest to assist in traffic navigation. Specifically, this thesis is concerned with finding the optimal placement of multiple ULiDs while adhering to roadway priority and LiDAR characteristic constraints. Some works have considered LiDAR placement under constraints; for instance, Lucic et al. [69] investigated the placement of ELiDs while adhering to the data requirements of the backhaul network. The optimized placement determined by Diels et al. [98] took into account the placement and mounting angles of LiDAR sensors on a UAV to maximize scanning and minimize vibrations, but the authors did not consider the placement of the UAV. Many other works have considered the placement of UAVs, though. For example, [79] and [82] optimized the placement of UAVs based on the communication needs of device users while considering transmission power constraints. Assi et al. [81] considered the optimal UAV placement to serve AV communication needs based on the age of information constraint. Ghazzai et al. [48] accounted for the joint placement of UAVs and their base

stations under multiple constraints (power, time of flight, and priority events). [99] discussed a similar UAV placement problem with similar constraints but formulated the problem with respect to roadside units and solar panels. [100] attempted to achieve optimal placement considering road priorities, but because their model utilized a camera instead of LiDAR, they could not consider LiDAR constraints. Ultimately, however, the author of this thesis is unaware of any studies that have attempted to optimally place multiple UAVs equipped with LiDAR sensors under road priority and LiDAR-specific constraints.

In this thesis, a novel ULiD placement framework under road priority and resolution requirements is proposed. The contributions of this thesis are summarized as follows:

- A placement optimization problem involving multiple ULiDs is formulated that maximizes the road coverage efficiency and considers the road priorities, LiDAR resolution quality, available number of ULiDs, and trajectory boundaries.
- Due to the non-convexity of the formulated problem, a PSO-based CI algorithm is proposed to solve the optimization problem.
- The proposed solution is investigated in environments with different road characteristics.
- Finally, the proposed solution is compared with other baselines to emphasize the advantages of the solution.

2. URBAN ROADWAY AND ULID SYSTEM MODEL

This section will describe the model of the designed system. Section 2.1 will outline the urban environment within which the ULiDs must operate. After the urban area is considered, the physical characteristics and limitations of the ULiD units will be explained in Section 2.2. Lastly, how the ULiDs interact with and observe the modeled urban environment will be examined in Section 2.3 in consideration of the ULiD characteristics.

2.1. ROADWAY CHARACTERISTICS

The urban environment has unique characteristics that must be considered when modeling this problem. Most importantly, for this problem, the road network is modeled as a traditional roadway grid in a dense, urban area with only straightaways, as shown in Figure 2.1. Modeling the network with only straight roads simplifies the process of modeling the ULiD coverage discussed later in this section. Since the roadways are straight and intersect only at 90° angles, the roadway can be broken up into smaller segments, $g \in \mathcal{G}$, and then modeled as squares. The center coordinates of each segment g are defined by $(x^g, y^g, 0) \in \mathbb{R}^3$, where the vertical coordinate z^g of each segment g is always zero because the ground is modeled as a flat plane. Each segment has identical side lengths of a; therefore, the area of each road segment equals $a^2 = A^g$.

Each roadway segment g may have concentrated areas of activity, e.g., intersections, busier roads, or areas occupied by traffic or accidents. Because these active segments represent more consequential data and thus are particularly relevant to the ULiD coverage area, an importance metric is introduced to represent segment activity: a continuous and normalized utility function, $I^g \in [0, 1]$. Values closer to 1 represent critical, busy, or risky segments, whereas values closer to 0 signify segments that are not as important. Each area A^g has an associated importance value I^g. Figure 2.2 shows one road layout used in the simulation, named Layout 1. Figure 2.2a shows a traditional view of Layout 1, while

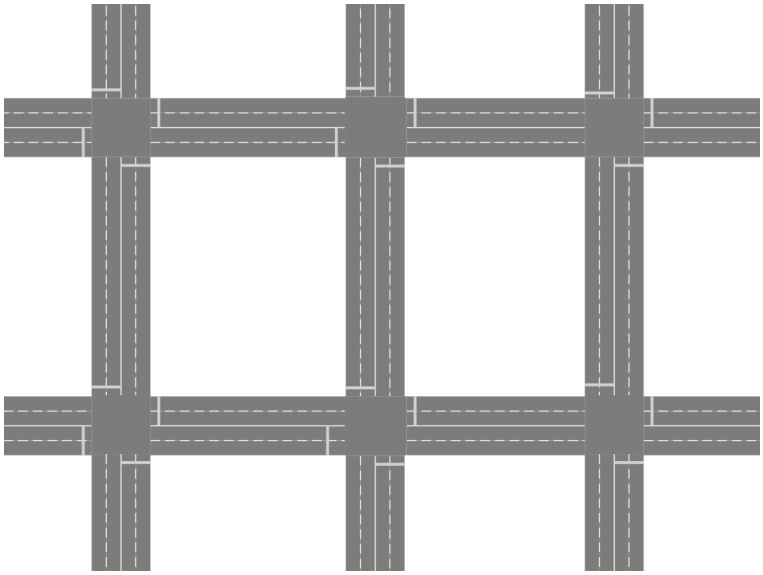

Figure 2.1. Traditional street grid.

Figure 2.2b shows the segmented representation and the color scale for the importance metric, I^g, for Layout 1. Each square box represents a segment. The colors are consistent with how I^g will be displayed throughout this thesis: darker colors signify relatively unimportant segments (with an importance value closer to 0), and lighter colors are more relevant segments with values closer to 1.

2.2. ULID CHARACTERISTICS

It is considered that a set of ULiDs $\lambda \in \Lambda$ operates above the roadways, and the maximum number of ULiDs that can be deployed may be based on either financial (budgetary) restrictions or available resource restrictions. The 3D coordinates associated with the location of a given ULiD are denoted $(x^\lambda, y^\lambda, z^\lambda) \in \mathbb{R}^3$, where x^λ and y^λ signify the locations of the ULiD parallel to the two orthogonal axes composing the flat ground plane and z^λ represents the ULiD's height above the ground (positive upward). It is assumed that all ULiDs have their LiDAR mounted on the underside of the UAV with their apertures always fixed parallel to the z axis and pointed in the negative z direction with an unobstructed

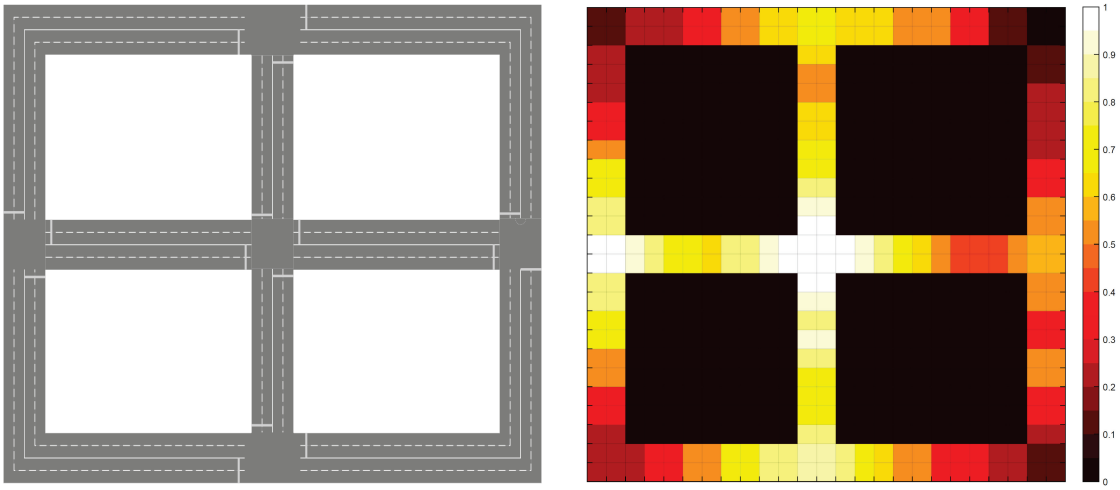

(a) Layout 1. (b) Layout 1 heat map.

Figure 2.2. Layout 1 as a grid and as a heat map.

view of the roadway. Therefore, there is no rotation of the ULiD about the x or y axes. However, a new variable, μ^{λ}, is introduced to represent the rotation of the ULiD about the z axis. Since the roadway is modeled as a grid with straight roads, the ULiD orientation about the z axis that maximizes coverage can be either 0° or 90°, which correspond to values of 0 or 1, respectively. Finally, the scan rate of a ULiD is denoted n^{λ}_{scan}, which represents the number of data points per second collected by the ULiD. It is common for LiDARs to be capable of capturing a variable number of data points without requiring them to alter their hardware [55, 56, 57]. Each ULiD can have a different n^{λ}_{scan}, but this value is set at the beginning of a flight and cannot be changed while the ULiD is in flight.

2.3. MODELING ULID COVERAGE

After accounting for the characteristics of the roadways and ULiDs, the FoV of the ULiD can be modeled. To align with current state-of-the-art LiDAR scanning patterns [55, 56, 57], the ULiDs are considered to adopt a horizontal scanning pattern, namely, a pattern comprising scans parallel to the x plane that move downward along the negative y axis. An

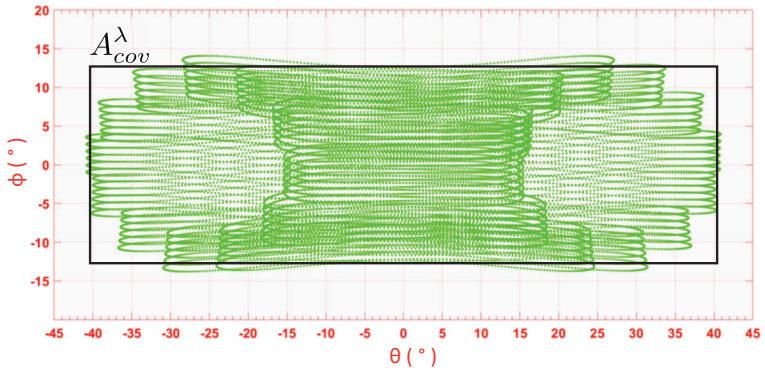

Figure 2.3. ULiD scan pattern [55].

example of the ULiD scan pattern is illustrated in Figure 2.3. All ULiDs have the same two FoV angles, θ and ϕ: θ is the maximum arc that the LiDAR can scan in the direction of flight (parallel to the roadway), and ϕ is similarly the maximum arc the LiDAR can scan from side to side (orthogonal to the direction of flight). The FoV angles are restricted by hardware limitations and cannot be altered during flight.

To simplify the system model, the area of a road segment scanned by a ULiD, A_{cov}^{λ} (hereafter referred to as the coverage area), is approximated as a rectangle (black rectangle in Figure 2.3). Figure 2.4 shows the same conceptual coverage area outlined in red and the area of a road segment outlined in blue. In this figure, H^{λ} represents the ground distance from the horizontal edge of the ULiD's FoV to the point on the road directly below the ULiD, and V^{λ} is the ground distance from the vertical edge of the ULiD's FoV to the point on the road directly below the ULiD. If the ULiD unit is rotated about the z axis by 90°, then μ^{λ} is equal to 1, and the ULiD coverage area is calculated as follows by swapping the values of θ and ϕ to account for the rotation:

$$A^{\lambda}_{cov} = 2(H^{\lambda}) * 2(V^{\lambda}), \tag{2.1a}$$

where

$$H^{\lambda} = z^{\lambda} \tan(\frac{\theta}{2}), \tag{2.1b}$$

$$V^{\lambda} = z^{\lambda} \tan(\frac{\phi}{2}). \tag{2.1c}$$

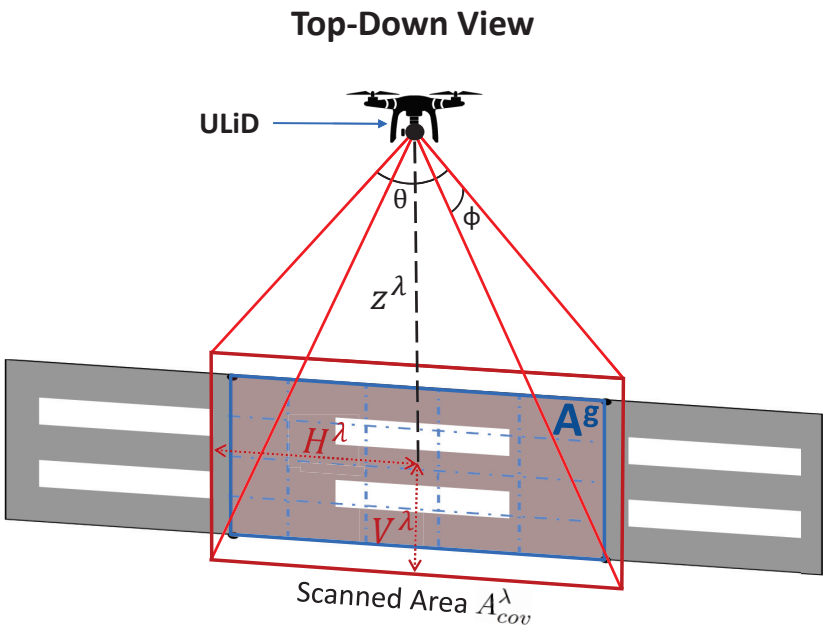

Figure 2.4. ULiD coverage of a road segment.

An important aspect of modeling the ULiD coverage area is the scan resolution, denoted R^{λ}, which is defined as the number of data points collected per second, n^{λ}_{scan}, per square meter. Defining this metric is crucial because an ITS application requires a certain standard within the data to detect and track objects [101]. In the described model, as the height of the ULiD increases, the coverage area increases, but n^{λ}_{scan} is fixed before the ULiD takes flight. Therefore, the resolution is inversely proportional to the covered area as follows:

$$R^{\lambda} = \frac{n^{\lambda}_{scan}}{A^{\lambda}_{cov}}. \tag{2.2}$$

3. ULID PLACEMENT PROBLEM FORMULATION

This section will formulate the placement optimization problem of multiple ULiDs with the goal of maximizing road coverage efficiency. Specifically, the problem seeks to maximize the weighted coverage area of a given road grid while minimizing the number of utilized ULiDs. Because this problem involves binary variables, it is non-convex and thus will be considered a mixed-integer nonlinear programming (MINLP) problem.

3.1. CONSTRAINTS

The system contains limitations that must be codified as constraints. These constraints are based on the physical characteristics of the system as well as the ITS data requirements.

3.1.1. Scannable Segment Constraint. In Section 2, a ULiD λ was defined to have a coverage area in the shape of a rectangle, and the roadways were broken up into square segments g, each having area A^g. A new variable, $\eta^{\lambda g}$, is introduced here to represent when an ULiD covers a road segment. $\eta^{\lambda g}$ is a binary variable: its value is 1 when the entire area of a segment is contained within the ULiD coverage area A^{λ}_{cov} and 0 if any of the segment's area lies outside of the coverage area. Therefore, $\eta^{\lambda g}$ can be expressed as:

$$\eta^{\lambda g} = \begin{cases} 1, \text{ if } \frac{a}{2} + \delta^g_x < H^\lambda \text{ and } \frac{a}{2} + \delta^g_y < V^\lambda \\ 0, \text{ otherwise} \end{cases}, \tag{3.1a}$$

where

$$\delta^g_x = |x^g - x^\lambda|, \tag{3.1b}$$

$$\delta^g_y = |y^g - y^\lambda|. \tag{3.1c}$$

3.1.2. Number of Available ULiDs Constraint. The ULiDs utilized in the problem space, ϵ^{λ}, cannot exceed the maximum number of available ULiDs, Λ, which may be based on financial (budgetary) restrictions or available resource restrictions. Therefore, the following constraint needs to be satisfied:

$$\sum_{\lambda} \epsilon^{\lambda} \leq \Lambda. \tag{3.2}$$

3.1.3. Resolution Constraint. Each road segment g has a minimum resolution of R^{g}_{min} based on the importance value of that segment. This minimum value is based on the requirements of the ITS system. A starting coefficient value established by the ITS, R_o, is multiplied by the importance to determine the minimum required resolution. The resolution provided by each ULiD, R^{λ}, must meet or exceed all R^{g}_{min} values within its FoV to count that covered segment, as shown below:

$$R^{\lambda} \geq \eta^{\lambda g} R^{g}_{min}, \ \forall \lambda \in \Lambda, \forall g \in G, \tag{3.3a}$$

where

$$R^{g}_{min} = R_o I^{g}, \ \forall g \in G. \tag{3.3b}$$

3.1.4. Problem Space Constraint. The problem space, $\mathbf{\Omega} \in \mathbb{R}^3$, is partially defined by the road grid's x and y coordinate boundaries. The placement of any ULiD outside of these boundaries would preclude the optimization problem from being solved (i.e., prevent any attempt to maximize the road coverage efficiency). In addition, the z axis problem space is limited insomuch that all ULiDs must fly above either a minimum height above the road or a maximum height outlined in the Federal Aviation Administration's UAV regulations.

Hence, the placement positions of the ULiDs must be within the solution space defined as:

$$(x^{\lambda}, y^{\lambda}, z^{\lambda}) \in \mathbf{\Omega},\ \forall \lambda \in \Lambda. \tag{3.4}$$

3.1.5. Unweighted Coverage Constraint. A final constraint, ξ_{min}, is introduced to ensure that the ULiDs cover a predetermined percentage of the urban road grid. In other words, this constraint guarantees that a minimum percentage of all road segments $g \in G$ is covered by the set of utilized ULiDs and is expressed as:

$$\frac{\sum_{g \in G} \eta^{\lambda g} A^{g}}{\sum_{g \in G} A^{g}} \geq \xi_{min}, \forall \lambda \in \Lambda. \tag{3.5}$$

3.2. MATHEMATICAL FORMULATION

The full optimization problem can be formulated with the problem's constraints codified above. The complete optimization problem ($\mathcal{P}$) is as follows:

$$(\mathcal{P}) \underset{x^{\lambda}, y^{\lambda}, z^{\lambda}, \mu^{\lambda}, \epsilon^{\lambda}}{\text{maximize}} \frac{\sum_{\lambda \in \Lambda} \sum_{g \in G} \eta^{\lambda g} A^{g} I^{g}}{\sum_{g \in G} A^{g} I^{g}} - E_o \sum_{\lambda \in \Lambda} \epsilon^{\lambda} \tag{3.6}$$

subject to

$$\eta^{\lambda g} \leq 1 - \frac{(\frac{a}{2} + \delta_x^g) - H^\lambda}{M}, \qquad \forall \lambda \in \Lambda,\ \forall g \in G, \tag{3.7a}$$

$$\eta^{\lambda g} > \frac{H^\lambda - (\frac{a}{2} + \delta_x^g)}{M}, \qquad \forall \lambda \in \Lambda,\ \forall g \in G, \tag{3.7b}$$

$$\eta^{\lambda g} \leq 1 - \frac{(\frac{a}{2} + \delta_y^g) - V^\lambda}{M}, \qquad \forall \lambda \in \Lambda,\ \forall g \in G, \tag{3.7c}$$

$$\eta^{\lambda g} > \frac{V^\lambda - (\frac{a}{2} + \delta_y^g)}{M}, \qquad \forall \lambda \in \Lambda,\ \forall g \in G, \tag{3.7d}$$

$$\sum_{\lambda \in \Lambda} \epsilon^\lambda \leq \Lambda, \tag{3.7e}$$

$$R^\lambda \geq \eta^{\lambda g} R_{min}^g, \qquad \forall \lambda \in \Lambda,\ \forall g \in G, \tag{3.7f}$$

$$(x^\lambda, y^\lambda, z^\lambda) \in \mathbf{\Omega}, \qquad \forall \lambda \in \Lambda, \tag{3.7g}$$

$$\frac{\sum_{g \in G} \eta^{\lambda g} A^g}{\sum_{g \in G} A^g} \geq \xi_{min}, \qquad \forall \lambda \in \Lambda. \tag{3.7h}$$

The first term in the objective function represents the weighted coverage percentage, and the second term represents a penalty for the energy consumed by the ULiDs. M is an arbitrarily large value, and E_o is a penalizing constant. As stated at the beginning of this section, the formulated optimization problem ($\mathcal{P}$) is an MINLP problem. In the next section, a CI-based solution for the designed problem will be proposed, and the results of its deployment will be evaluated.

4. ULID PLACEMENT SOLUTION

This section will describe the PSO algorithm developed to solve the MINLP problem presented in Section 3.2. It will then explain the deployment of this algorithm and discuss the simulation results.

4.1. COMPUTATIONAL INTELLIGENCE ALGORITHM

As mentioned in Section 1.4, PSO algorithms boast a number of properties that make them especially useful for solving nonlinear problems. Consequently, this thesis deployed a PSO-based CI algorithm to solve the proposed MINLP problem. PSO algorithms typically share a few key design elements, beginning with the initialization of a population that then searches iteratively for the optimal solution based on its current fitness; then, its fitness updates as the population moves throughout the iterations; finally, the algorithm terminates its search after completing a certain number of iterations or fulfilling a predetermined condition. This general structure is schematically represented by the flow chart in Figure 4.1.

The PSO algorithm designed for this MINLP problem starts with a set number of particles, i.e., the population in the solution space, $npop$. Each particle in the population represents one possible ULiD placement solution and is initialized at a random location, $lo(i)$, with zero velocity, $ve(i)$. The optimization problem is evaluated as the cost, $cost$, using the particle's location while adhering to the designed constraints. The particles then begin to iteratively search for the maximum cost, and while doing so, each particle remembers both its personal best location and cost, $b_{lo}(i)$ and $b_{co}(i)$, respectively, and the global best location and cost, $iterative.best.lo$ and $iterative.best.co$, respectively. Each particle's velocity, $ve(i)$, is updated at the start of each iteration using knowledge of that particle's best location, the global best location, and the particle's last velocity as

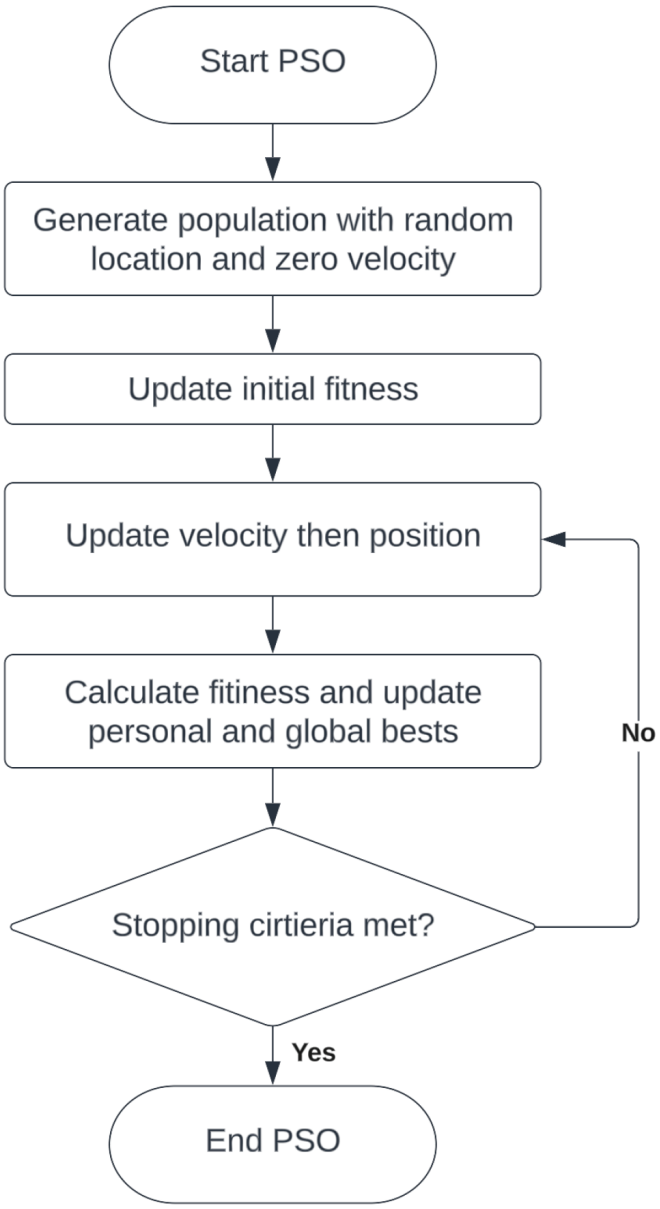

Figure 4.1. Flow chart of a generic PSO algorithm.

follows [43]:

$$ve(i) = w * ve(i) + c_1 * r_p\Big(b_{lo}(i) - lo(i)\Big) + c_2 * r_p\Big(iterative.best.lo - lo(i)\Big), \quad (4.1a)$$

where

$$w = (w_1 - w_2) * (1 - \frac{t}{maxit}). \quad (4.1b)$$

In the above update equation, c_1 and c_2 are the personal and global learning coefficients, respectively; r_p is a random positive number; the current particle and current iteration are given as i and t, respectively; the integer value denoting the number of iterations over which the particles are evaluated is $maxit$; and w denotes the inertia weight, with w_1 and w_2 being set values that determine the range of inertia weights. The inertia weight is updated every iteration via a modified version of the linearly varying inertia weight model [44], which enables an early global search (exploration) to adapt into a local search (exploitation) towards the end of the iterative process. The location of each particle i is updated every iteration by the following:

$$lo(i) = lo(i) + ve(i). \quad (4.2)$$

As mentioned above, each particle represents one possible ULiD location. Once the PSO algorithm has finished iterating, a single location, namely, the best calculated ULiD position, is returned. It follows, then, that because this algorithm yields only a single ULiD placement, the PSO algorithm must be executed a number of times to achieve the goal, which is to determine the optimal placement positions of multiple ULiDs. After each PSO iteration, a new ULiD position is added to the total cumulative output values, which are updated with each addition. The urban environment is likewise updated to reflect the

newly determined ULiD placement by setting the importance values, I^g, for all of the road segments covered by the newest ULiD to 0; these road segments are represented by the variable $\eta^{\lambda g}$. Updating these values to 0 serves both to reduce the overlapping area covered by the ULiDs and to further maximize the total number of segments covered within the urban environment. The PSO algorithm iteratively places one ULiD at a time until the unweighted coverage constraint (3.7h) is met. To complete this process, the PSO algorithm requires as input only the simulation parameters, collectively denoted $SimParameters$, which consist of the roadway and ULiD characteristics described in Section 2 and will be assigned values in the next section. The pseudocode for the implemented PSO algorithm is given in Algorithm 38.

A subset objective problem, named the weighted coverage problem, $\mathcal{P}1$, is extracted from $\mathcal{P}$ to account for the cost function in the simulated problem. This change is due to the discrete variable representing the number of utilized ULiDs, ϵ^λ, in the optimization problem. Since the PSO algorithm is executed iteratively, it is not possible to reduce ϵ^λ or to alter a ULiD's position once its placement has been selected. The problem $\mathcal{P}1$ does not penalize the system for a new ULiD placement since the PSO algorithm cannot optimize that portion of problem $\mathcal{P}$. The subset objective problem is defined as:

$$(\mathcal{P}1) \underset{x^\lambda, y^\lambda, z^\lambda, \mu^\lambda}{\text{maximize}} \frac{\sum_{\lambda\in\Lambda}\sum_{g\in G}\eta^{\lambda g}A^g I^g}{\sum_{g\in G}A^g I^g}, \tag{4.3}$$

subject to (3.7a) - (3.7d), (3.7f) - (3.7h).

4.2. SIMULATION RESULTS

This section presents selected simulation results to validate the proposed PSO algorithm. The urban area of interest is assumed to be 250 $m \times 250$ m, and the UAV flight domain is given as $\mathbf{\Omega} \in ([0, 250], [0, 250], [20, 200])$. The simulation parameters define the urban environment and ULiD characteristics, the default values of which are defined in

Algorithm 1: Proposed PSO Algorithm

Input: SimParameters
Initialization:
ULiD = 0;
Iterative PSO Loop:
while *Unweighted Coverage* $< \xi_{min}$ **do**
    ULiD = ULiD + 1;
    iterative(ULiD).best.co = -inf;
    iterative(ULiD).best.lo = [];
    for *i = 1:npop* **do**
        lo(i)=unifrnd(Ω_{min}, Ω_{max}, varsize);
        ve(i)=zeros(varsize);
        b_{co}(i)=costfunction(lo(i));
        b_{lo}(i)=lo(i);
        if b_{co}*(i) > iterative(ULiD).best.co* **then**
            iterative(ULiD).best.co = b_{co}(i);
            iterative(ULiD).best.lo = b_{lo}(i);
        end
    end
    for *t = 1:maxit* **do**
        Update inertia coefficient.
        for *i = 1:npop* **do**
            Update the velocity and location of particle i (4.1),(4.2)
            if *lo(i)* $< \Omega_{min}$ **then**
                $lo(i) = \Omega_{min}$;
            else if *lo(i)* $> \Omega_{max}$ **then**
                $lo(i) = \Omega_{max}$;
            end
            cost=costfunction(lo(i));
            if *cost* > b_{co}*(i)* **then**
                b_{co}(i) = cost;
                b_{lo}(i) = lo(i);
            end
            if b_{co}*(i) > iterative(ULiD).best.co* **then**
                iterative(ULiD).best.co = b_{co}(i);
                iterative(ULiD).best.lo = b_{lo}(i);
            end
        end
    end
    iterative(ULiD) = outputCalculations();
    OutputTotal = [OutputTotal; iterative(ULiD)];
end

Table 4.1a unless otherwise specified. The parameters a, θ, ϕ, and n^{λ}_{scan} were set to realistic values [55], while R_o and ξ_{min} were assigned arbitrarily. The values of the PSO parameters (shown in Table 4.1b), which dictate how the PSO algorithm is executed, were chosen because they have previously been shown to yield positive PSO outcomes [44]. Layout 1, first described in Section 2.1, was simulated as the default layout for all scenarios except those discussed in Section 4.2.1.

Table 4.1. Simulation and PSO parameters

(a) Simulation parameters.

Parameter	Value
a	$10\ m$
θ	$81.7°$
ϕ	$25.1°$
n^{λ}_{scan}	$480k\ pts/s$
R_o	$250\ pts/s * m^2$
ξ_{min}	80%

(b) PSO parameters.

Parameter	Value
$npop$	20
$maxit$	250
c_1	1.496
c_2	1.496
w_1	0.8
w_2	1.4

4.2.1. ULiD Placements in Different Urban Layouts. This section presents the simulated ULiD placement positions corresponding to four distinct urban layouts, as shown in Figure 4.2. The colors of the segments represent the I^g values, where lighter colors represent larger I^g values, i.e, more important road segments. The different urban layouts were assigned different I^g distributions to test the effective placements of the ULiDs. Each 'X' marker represents the (x^{λ}, y^{λ}) position of a ULiD, and the colored rectangles (denoted "FoV Outline N", with N being an integer matching the FoV to its ULiD) show the boundaries of the corresponding FoV, A^{λ}_{cov}. Segments contained entirely inside a ULiD's FoV are the segments covered by the ULiD marked with an 'X' of the same color. The higher the altitude z^{λ} at which a ULiD flies, the greater the area A^{λ}_{cov} the ULiD can cover and thus the larger the FoV outline of that ULiD.

According to Figure 4.2a, the PSO algorithm utilized 12 ULiD units to achieve a minimum percentage ξ_{min} of 80%. Furthermore, half of the ULiDs were rotated 90° to better cover the roads paralleling the y axis. Layouts 2 and 3, shown in Figure 4.2b and 4.2c, respectively, each required only 8 ULiDs to satisfy the ξ_{min} constraint. These two layouts had $\approx$ 2% fewer segments than did Layout 1 but utilized 4 fewer ULiD units. This significant reduction in the number of utilized ULiD units is attributed both to the layout of the road segments and to the larger I^g values being more centralized than those in Layout 1. In other words, the segments were closer together, which meant that a single ULiD could cover more ground, resulting in fewer utilized ULiDs. In addition, Layout 4 (Figure 4.2d) had $\approx$ 20% more segments than Layout 1 but utilized 2 fewer ULiD units; this result is attributed to Layout 4 having more centralized segments and larger I^g values than Layout 1. Ultimately, the placement and rotation of the ULiD units for each of the four simulated layouts are appropriate.

4.2.2. ULiD Placement Details for Layout 1. The ULiD placements from Layout 1 are examined below. The legend shown in Figure 4.3b is used for both sub-figures, and the colors correlate with those used in Figure 4.2a to identify the ULiDs. Figure 4.3a shows the initial ULiD placements (drawn as circles) at the beginning of a PSO iteration and the final ULiD placements (drawn as 'X' markers) at the end of a PSO iteration. The like-colored line connecting each pair of initial and final placement markers shows the path that ULiD took throughout its PSO iteration. The algorithm placed ULiDs 1 through 11 at altitudes between 48 and 70 meters to optimally cover the segments within its FoV and provide the required R^g_{min}. ULiD 12 was the only unit placed above 70 meters, which occurred because the unit covers segments with low R^g_{min} values. Figure 4.3b reveals a total weighted coverage value of 87.31% for Layout 1 calculated using cost function $\mathcal{P}1$ and demonstrates how the individual weighted coverage of each ULiD contributed to the total weighted coverage of the system. As more ULiDs populated the problem space, the number of available optimal

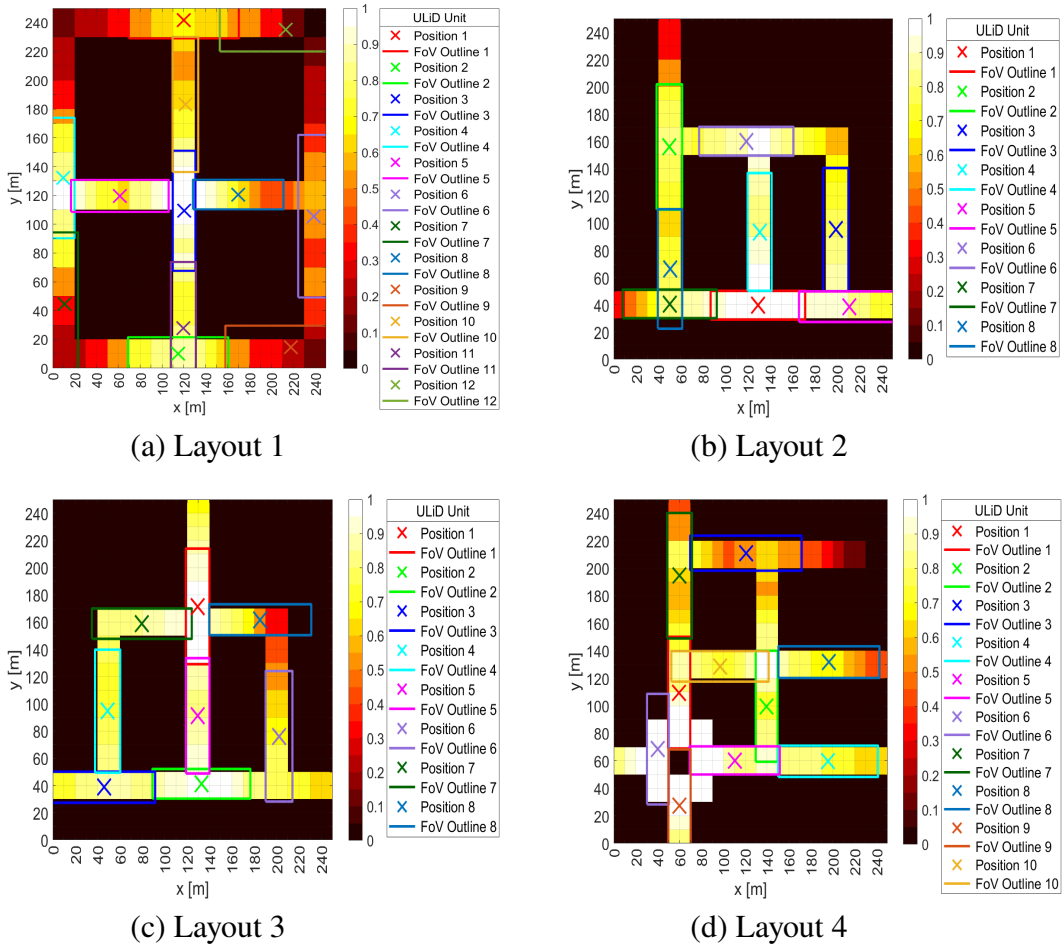

(a) Layout 1

(b) Layout 2

(c) Layout 3

(d) Layout 4

Figure 4.2. ULiD placement heat maps for four distinct urban layouts.

placement positions diminished, which resulted in later-placed ULiDs contributing less to the weighted coverage. The results of this simulation are logical and consistent with the expected outcome.

4.2.3. Effects of Changing R_o with Different ξ_{min}. Each segment has a minimum resolution, R^g_{min}, that a ULiD must provide to properly cover that segment. This minimum resolution is computed by multiplying the coefficient R_o by I^g. R_o was statically set for the previous simulations, but for this section, the value was altered to investigate how it affects the number of utilized ULiDs. As stated earlier, the resolution provided by a ULiD, R^λ, is based on the height of its placement. Thus, larger values of R_o should require ULiDs

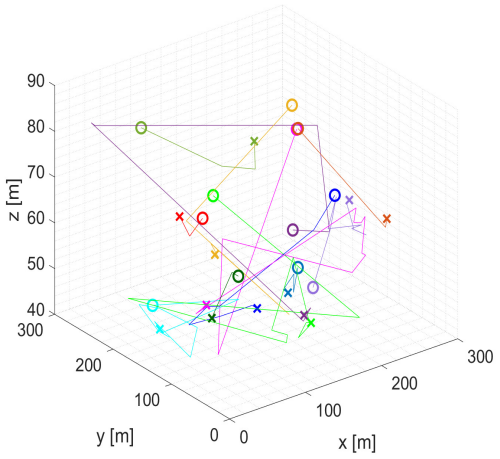

(a) ULiD search paths during the PSO iterations. Circles represent the starting 3D positions of the ULiDs, while the 'X' markers represent their final 3D positions.

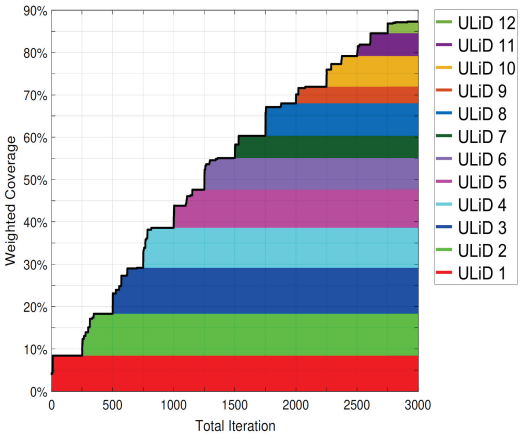

(b) Weighted coverage versus total iterations of the PSO algorithm. The colors of the horizontal bars correspond to the different ULiD units, and the size reflects each ULiD's contribution to the total weighted coverage.

Figure 4.3. ULiD search paths and individual contributions to the total weighted coverage for Layout 1.

to be placed at lower altitudes to satisfy the constraint (3.7f). Additionally, since a lower flight altitude would mean that a ULiD cannot cover as many segments, a larger R_o should require more ULiDs to be utilized to satisfy the stopping criterion ξ_{min}, which is defined as the unweighted coverage constraint that requires the entire set of utilized ULiD units to cover a certain percentage of the total segments in the urban layout. Accordingly, larger values of ξ_{min} are expected to correspond to a greater number of utilized ULiDs.

Figure 4.4 shows the required number of ULiD units for different R_o values. R_o was simulated with values of 100, 200, 300, and 400, each of which was simulated with ξ_{min} set to 60%, 70%, 80%, and 90% (plotted as the four lines in the graph). As expected, when the value of R_o increased, more ULiD units were needed to meet the minimum resolution constraint. In addition, a positive correlation was expected between ξ_{min} and R_o, and the figure indicates that this prediction was true; however, the 80% and 90% lines overlap at R_o values of 100 and 200. This overlap is attributed to the stochastic nature of the PSO

algorithm. Nevertheless, because the trends of the curves (based on ξ_{min}) are all fairly linear, a middle-ground R_o value of 250 $pts/s * m^2$ was chosen as the baseline for the other simulations.

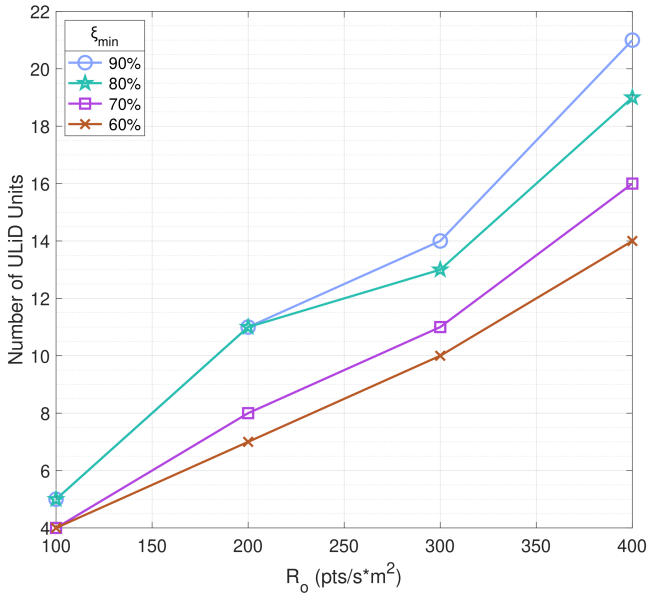

Figure 4.4. Number of ULiDs versus R_o with different ξ_{min} values.

4.2.4. Effects of Changing n^{λ}_{scan} with Different ξ_{min}. The ULiDs are all assumed have a fixed scan rate, n^{λ}_{scan}, during each execution of the PSO algorithm. This parameter defines how many points the ULiD collects per second using its LiDAR sensor. n^{λ}_{scan} directly affects the ULiD's resolution, R^{λ}, defined as the number of data points per second per square meter. A faster scan rate allows the ULiDs to meet the R^{g}_{min} requirements from higher altitudes, while a slower scan rate requires the unit to position itself at a lower altitude, thus requiring more ULiDs to meet the ξ_{min} constraint.

The scan rate was set to five values, $100k$, $200k$, $300k$, $400k$, and $500k$ pts/s, to test the number of ULiD units required to meet two values of ξ_{min}, 60% and 80%. The results for these simulations are shown in Figure 4.5. The two color bars are the two tested values of ξ_{min}, and the five groups of bars represent the five different n^{λ}_{scan} values. When the scan rate was set to $100k$ pts/s with ξ_{min} equal to 80%, the PSO algorithm placed 43 ULiD units to meet the constraints. With the same scan rate at ξ_{min} equal to 60%, the number of

required units decreased to 32. Thus, a 20% decrease in ξ_{min} resulted in a 26% decrease in the number of utilized ULiDs. However, when the scan rate was set to the maximum value of $500k\ pts/s$, the numbers of utilized ULiDs were 11 and 9 when ξ_{min} was set to 80% and 60%, respectively. In this case, the 20% decrease in ξ_{min} resulted only in an 18% decrease in the number of utilized ULiDs. These results show that as the ULiD scan rate rises, the ξ_{min} requirement has a diminishing effect on the number of utilized ULiD units.

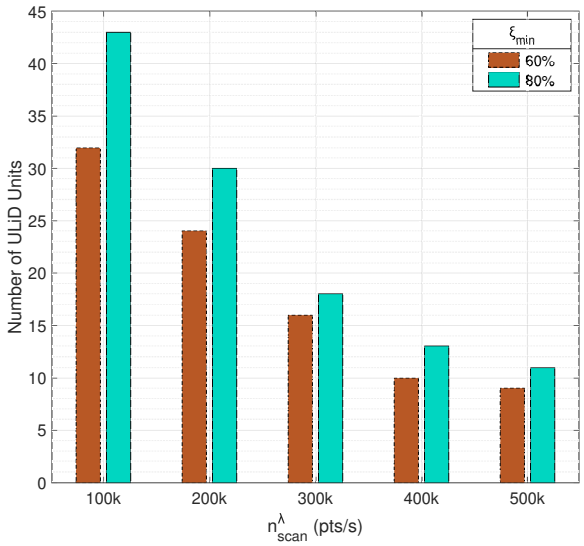

Figure 4.5. Number of ULiD units versus n^{λ}_{scan}.

4.2.5. PSO Algorithm versus Two Baseline Placements Using Monte Carlo. In this section, the PSO algorithm is compared with two baseline placement methods: the first utilizes a uniform placement distribution to deploy a set number of ULiDs, while the second uses a random Gaussian distribution to select ULiD placements. A Monte Carlo simulation was performed with 1000 trials, and every trial generated 15 ULiD positions with the appropriate random distribution. The weighted coverage cost function was calculated for each of the 15 ULiD positions. After the 1000 trials of 15 randomly placed ULiDs, the trials were averaged so that a single weighted coverage was given for each of the 15 simulated ULiDs. The random placement algorithms employed the same method, and both baseline placements followed the same constraints as those listed in $\mathcal{P}1$. The PSO algorithm was

manually simulated with the default parameters for 1 to 15 ULiD units. It should be noted that it was unnecessary to perform multiple PSO trials because the algorithm inherently conducts an iterative searching process.

The weighted coverage values yielded by the three placement methods are plotted versus the number of utilized ULiDs in Figure 4.6. Note that the y axis is a logarithmic scale; this scale was used because the PSO algorithm greatly outperformed the two random placement methods. The PSO algorithm approached a weighted coverage value of 95% when placing 15 ULiD units compared to the value of ≈4.5% that both random placement methods achieved with 15 units. In addition, the first ULiD unit placed using the PSO algorithm had a weighted coverage of ≈11%. Ultimately, the value for a single placed ULiD using the PSO algorithm was greater than twice the total weighted coverage for 15 ULiDs using either of the two random placement methods.

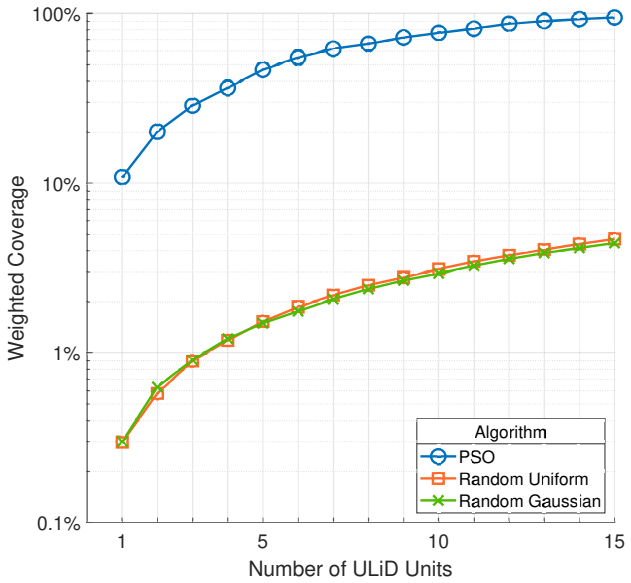

Figure 4.6. Weighted coverage versus number of ULiD units with different placement algorithms.

5. CONCLUSIONS

This thesis explained how urbanization amplifies the need for improved transportation infrastructure by exacerbating traffic congestion and leads to multiple public safety concerns: vehicle accidents, environmental pollution, and issues with emergency response management. Research into ITS may hold the critical key that will inevitably remedy the described problems, but many possible solutions exist within this field. The public sector has historically been responsible for developing and deploying ITS technologies, but recent technological advancements have allowed the private sector to contribute their own solutions. Among the most helpful and widely distributed ITS solutions are privately created GPS-enabled navigation applications, which utilize AI algorithms to help improve navigation suggestions; nevertheless, the techniques used to collect the data with which to train these AI algorithms are inadequate due to the disconnect between the public and private ITS sectors.

Consequently, researchers have long focused on methods to increase the efficiency of data collection for public ITS. LiDAR has emerged as a leading data acquisition technique; LiDAR sensors can generate highly precise 3D maps, thereby enabling real-time object detection and tracking, which can be used for traffic navigation and management in ITS. However, LiDAR sensors are notably expensive and generate vast volumes of data. Hence, reducing the number of sensors and maximizing their potential is a considerable field of interest. Some scholars have suggested moving LiDAR sensors from autonomous vehicles to elevated positions along roadways, but this solution is still insufficient: the fixed placement of LiDAR sensors still limits the sensors' FoVs and necessitates using an excessively large number of sensors. In contrast, ULiDs have been used for decades to deploy sensors with an aerial vantage point to capture data. Unfortunately, due to the limitations of wireless communications, these ULiDs have been unable to communicate data in real time for

ITS purposes. Nevertheless, inevitable improvements to communication networks and the development of 6G will eventually enable real-time ULiD data acquisition for ITS applications.

Accordingly, this thesis formulated a placement optimization problem involving multiple ULiD units with the goal of maximizing their road coverage efficiency while considering spatial and LiDAR-specific constraints, road coverage priorities, and scanning resolution requirements. Due to the non-convexity of the formulated problem, a PSO-based CI algorithm was proposed to solve the problem. Simulations demonstrated that the developed PSO algorithm was robustly capable of efficiently placing multiple ULiD units in different road layout scenarios. These results were further confirmed when the PSO algorithm greatly outperformed two baseline algorithms.

Research in ITS, particularly the utilization and placement of LiDAR sensors, is expected to accelerate. Consequently, future work will expand upon this thesis to investigate a more complex system model and more intelligent algorithm. The author of this thesis intends to model a dynamic road and traffic scenario to analyze the effects of a changing importance factor on the dynamic placement of multiple ULiDs. More variables will also be considered, such as the rotation of the LiDAR sensor and the energy requirements of the ULiDs. Moreover, to solve a more complex system, a more sophisticated algorithm will be utilized. Nevertheless, the algorithm proposed herein is part of the RL field of AI algorithms and will be well-suited to handle the increased difficulty of such systems.

REFERENCES

[1] The World Bank Group, "Urban development - overview," Oct. 2022.

[2] H. Ritchie and M. Roser, "Urbanization," *Our World in Data*, Sep. 2018.

[3] United Nations, "Global issues: Population," 2022.

[4] A. R. Foxx, J. A. V. N. T. S. C. (U.S.), and U. S. D. of Transportation. Office of the Under Secretary for Policy, "Beyond traffic: 2045 final report," Jan. 2017.

[5] United States Census Bureau, "Census bureau estimates show average one-way travel time to work rises to all-time high," *United States Census Bureau*, Mar. 2021.

[6] A. Push, "How the american commute has changed over the past 50 years," Jun. 2022.

[7] United States Census Bureau, *Travel Time to Work in the United States: 2019*. United States Census Bureau, Mar. 2021.

[8] World Health Organization, *Global status report on road safety 2018*. Genève, Switzerland: World Health Organization, Jun. 2018.

[9] M. Wayland, "More people are dying on u.s. roads, even as cars get safer. here's why it's a tough problem to solve," May 2022.

[10] United States Environmental Protection Agency, "Climate change indicators: Greenhouse gases," Aug. 2022.

[11] National Oceanic and Atmospheric Administration, "Climate change impacts," Aug. 2021.

[12] K. Hayhoe, J. Edmonds, R. E. Kopp, A. N. LeGrande, B. M. Sanderson, M. F. Wehner, and D. J. Wuebbles, *Climate Models, Scenarios, and Projections*, pp. 133–160. Washington, D.C.: U.S. Global Change Research Program, 2017.

[13] National Geographic Staff, "The environmental impacts of cars, explained," Sep. 2019.

[14] D. Brent and L. Beland, "Traffic congestion, transportation policies, and the performance of first responders," *Journal of Environmental Economics and Management*, vol. 103, p. 102339, Sep. 2020.

[15] R. Griffin and G. J. McGwin, "Emergency medical service providers' experiences with traffic congestion," *The Journal of emergency medicine*, vol. 44, pp. 398–405, Feb. 2013.

[16] A. Castillo, "Increase in emergency response time caused by insufficient staffing, traffic congestion," Aug. 2022.

[17] World Meteorological Organization, "Weather-related disasters increase over past 50 years, causing more damage but fewer deaths," Aug. 2021.

[18] T. Frank, "Disasters displaced more than 3 million americans in 2022," Feb. 2023.

[19] L. Thompson, "Natural disasters, boosted by climate change, displaced millions of people in u.s. in 2022," Feb. 2023.

[20] A. Auer, S. Feese, S. Lockwood, and A. Vann Easton, "History of intelligent transportation systems: 2021 update.," Nov. 2021. Tech Report, FHWA-JPO-16-329.

[21] A. Pariona, "What was the digital revolution?," Apr. 2017.

[22] S. Shaheen and R. Finson, "Intelligent transportation systems," Dec. 2013.

[23] M. Tubaishat, P. Zhuang, Q. Qi, and Y. Shang, "Wireless sensor networks in intelligent transportation systems," *Wireless Communications and Mobile Computing*, vol. 9, pp. 287–302, Mar. 2009.

[24] M. Choudhary, "What is intelligent transport system and how it works?," Jan. 2019.

[25] S. Chan-Edmiston, S. Fischer, S. Sloan, and M. Wong, "Intelligent transportation systems (its) joint program office: Strategic plan 2020–2025," Mar. 2020. Tech Report FHWA-JPO-18-746.

[26] Kimley-Horn and Associates, Inc., "Executive summary of the bay area its architecture," Apr. 2021.

[27] Technavio Research, "Global intelligent transport system (its) market 2020-2024," Apr. 2020.

[28] T. Homer, "How traffic lights detect cars are waiting for the light to change," Jan 2023.

[29] T. Mai, "Global positioning system history," Aug 2017.

[30] G. de Boer, "The history of navigation and what's next," Oct. 2020.

[31] J. P. Leite, "A brief history of gps in-car navigation," Nov. 2021.

[32] A. He, "People continue to rely on maps and navigational apps," Jul. 2019.

[33] Car Pro, "Where drivers are most dependent on gps systems," Mar. 2022.

[34] AppMagic, "Leading mapping apps in the united states in 2022, by downloads," Feb. 2023.

[35] M. DeGeurin, "Google's maps looks to solidify its navigation dominance with ai-powered tools," Mar. 2021.

[36] R. Koch, "How ai in traffic management is helping to ease traffic congestion," Jul. 2022.

[37] B. Pericolosi, "How google maps platform uses ai/ml and community contributions to keep its points of interest up to date," Dec. 2022.

[38] J. McCarthy, "What is artificial intelligence?," *The Stanford Formal Reasoning Group*, Nov. 2007.

[39] C. Smith, B. McGuire, T. Huang, and G. Yang, "The history of artificial intelligence," Dec. 2006.

[40] N. Siva, "Artificial intelligence (ai) vs. machine learning vs. deep learning," Jun. 2019.

[41] IEEE Computational Intelligence Society, "What is computational intelligence?," 2023.

[42] J. C. Bezdek, "Computational intelligence defined - by everyone !," in *Computational Intelligence: Soft Computing and Fuzzy-Neuro Integration with Applications* (O. Kaynak, L. A. Zadeh, B. Türkşen, and I. J. Rudas, eds.), (Berlin, Heidelberg), pp. 10–37, Springer Berlin Heidelberg, 1998.

[43] J. Kennedy and R. Eberhart, "Particle swarm optimization," in *Proceedings of ICNN'95 - International Conference on Neural Networks, Perth, WA, Australia*, Nov. 1995.

[44] T. Shami, A. El-Saleh, M. Alswaitti, Q. Al-Tashi, M. A. Summakieh, and S. Mirjalili, "Particle swarm optimization: A comprehensive survey," *IEEE Access*, vol. 10, pp. 10031–10061, Jan. 2022.

[45] A. Alsharoa, H. Ghazzai, and M.-S. Alouini, "Near-optimal power allocation with pso algorithm for mimo cognitive networks using multiple af two-way relays," in *Proceedings of the IEEE International Conference on Communications, Sydney, Australia*, pp. 1580–1584, Jun. 2014.

[46] X. Zhen, Z. Enze, and C. Qingwei, "Rotary unmanned aerial vehicles path planning in rough terrain based on multi-objective particle swarm optimization," *Journal of Systems Engineering and Electronics*, vol. 31, pp. 130–141, Feb. 2020.

[47] H. Shakhatreh, A. Khreishah, A. Alsarhan, I. Khalil, A. Sawalmeh, and N. S. Othman, "Efficient 3d placement of a uav using particle swarm optimization," in *2017 8th International Conference on Information and Communication Systems, Irbid, Jordan*, pp. 258–263, Apr. 2017.

[48] H. Ghazzai, H. Menouar, A. Kadri, and Y. Massoud, "Future uav-based its: A comprehensive scheduling framework," *IEEE Access*, vol. 7, pp. 75678–75695, Jun. 2019.

[49] A. Thevenot, "Particle swarm optimization (pso) visually explained," Dec. 2020.

[50] J. Macfarlane, "When apps rule the road: The proliferation of navigation apps is causing traffic chaos. it's time to restore order," *IEEE Spectrum*, vol. 56, pp. 22–27, Sep. 2019.

[51] S. Monogios, K. Limniotis, N. Kolokotronis, and S. Shiaeles, "A case study of intra-library privacy issues on android gps navigation apps," in *E-Democracy – Safeguarding Democracy and Human Rights in the Digital Age* (S. Katsikas and V. Zorkadis, eds.), pp. 34–48, Springer International Publishing, Dec. 2019.

[52] United States Army Special Operations Command, "Consumer privacy & identity quarterly," *USASOC Identity Management*, Sep. 2017.

[53] National Oceanic and Atmospheric Administration, "What is lidar?," Jan. 2023.

[54] GISGeography, "A complete guide to lidar: Light detection and ranging," Aug. 2022.

[55] Livox Technology Company Limited, *Livox Horizon User Manual*, 1.0 ed., Oct. 2019. Accessed: 10-29-2021.

[56] Ouster, Inc., *OS0 Datasheet*, rev7 ed., Jul. 2022. Accessed: 02-26-2023.

[57] Velodyne LiDAR, Inc., *VLP-16 User Manual*, 63-9243 rev. e ed., Feb. 2019. Accessed: 02-26-2023.

[58] E. Guizzo, "How google's self-driving car works," Oct. 2011.

[59] P.-Y. Kong, "Computation and sensor offloading for cloud-based infrastructure-assisted autonomous vehicles," *IEEE Systems Journal*, vol. 14, pp. 3360–3370, Sep. 2020.

[60] T. Luettel, M. Himmelsbach, and H.-J. Wuensche, "Autonomous ground vehicles—concepts and a path to the future," *Proceedings of the IEEE*, vol. 100, pp. 1831–1839, May 2012.

[61] J. B. Martirena, M. N. Doncel, A. C. Vidal, O. O. Madurga, J. F. Esnal, and M. G. Romay, "Automated annotation of lane markings using lidar and odometry," *IEEE Transactions on Intelligent Transportation Systems*, vol. 23, pp. 3115–3125, Apr. 2022.

[62] H. Wei and M. Huang, "Intelligent vehicle positioning method based on gps/lidar/derivative data fusion," in *2020 IEEE 3rd International Conference on Information Systems and Computer Aided Education, Dalian, China*, pp. 153–157, Sep. 2020.

[63] F. Ghallabi, G. El-Haj-Shhade, M.-A. Mittet, and F. Nashashibi, "Lidar-based road signs detection for vehicle localization in an hd map," in *2019 IEEE Intelligent Vehicles Symposium, Paris, France*, pp. 1484–1490, Aug. 2019.

[64] F. Ghallabi, M.-A. MITTET, G. EL-HAJ-SHHADE, and F. Nashashibi, "Lidar-based high reflective landmarks (hrl)s for vehicle localization in an hd map," in *2019 IEEE Intelligent Transportation Systems Conference, Auckland, New Zealand*, pp. 4412–4418, Oct. 2019.

[65] S. Liu, J. Tang, Z. Zhang, and J.-L. Gaudiot, "Computer architectures for autonomous driving," *Computer*, vol. 50, pp. 18–25, Aug. 2017.

[66] R. Wu, Z. Chowdhury, G. V. Sanchez, X. Gao, C. Villa, and X. Jiang, "Real-time vehicle detection system for intelligent transportation using machine learning," in *2022 IEEE Green Energy and Smart System Systems, Long Beach, CA, USA*, pp. 1–6, Nov. 2022.

[67] S. Kim, J. Ha, and K. Jo, "Semantic point cloud-based adaptive multiple object detection and tracking for autonomous vehicles," *IEEE Access*, vol. 9, pp. 157550–157562, Nov. 2021.

[68] D. Jung and D. Park, "Accelerated on-chip algorithm based on semantic region-based partial difference detection for lidar-vision depth data transmission reduction in lightweight controller systems of autonomous vehicle," in *2021 IEEE 14th International Symposium on Embedded Multicore/Many-core Systems-on-Chip, Singapore, Singapore*, pp. 16–22, Dec. 2021.

[69] M. C. Lucic, H. Ghazzai, and Y. Massoud, "Elevated lidar placement under energy and throughput capacity constraints," in *2020 IEEE 63rd International Midwest Symposium on Circuits and Systems, Springfield, MA, USAF*, pp. 897–900, Aug. 2020.

[70] M. C. Lucic, H. Ghazzai, A. Alsharoa, and Y. Massoud, "A latency-aware task offloading in mobile edge computing network for distributed elevated lidar," in *IEEE International Symposium on Circuits and Systems, Sevilla, Spain*, pp. 1–5, Oct. 2020.

[71] N. Jayaweera, N. Rajatheva, and M. Latva-aho, "Autonomous driving without a burden: View from outside with elevated lidar," in *2019 IEEE 89th Vehicular Technology Conference, Honolulu, HI, United States*, Apr. 2019.

[72] M. Padmal, D. Marasinghe, V. Isuru, N. Jayaweera, S. Ali, and N. Rajatheva, "Elevated lidar based sensing for 6g - 3d maps with cm level accuracy," in *2022 IEEE 95th Vehicular Technology Conference, Helsinki, Finland*, pp. 1–5, Aug. 2022.

[73] G. Coppola and E. Dey, "Driverless cars are giving engineers a fuel economy headache," Oct. 2017.

[74] I. Maksymova, C. Steger, and N. Druml, "Review of lidar sensor data acquisition and compression for automotive applications," in *Eurosensors Conference 2018, Graz, Austria*, Sep. 2018.

[75] E. Darack, "A brief history of quadrotors," *Smithsonian Magazine: Air & Space Magazine*, May 2019.

[76] K. Vyas, "A brief history of drones: The remote controlled unmanned aerial vehicles (uavs)," Jun. 2020.

[77] P. Posea, "The complete history of drones (1898 - 2021)," 2021.

[78] A. Alsharoa and M. Yuksel, "Uav-direct: Facilitating d2d communications for dynamic and infrastructure-less networking," in *DroNet'18: Proceedings of the 4th ACM Workshop on Micro Aerial Vehicle Networks, Systems, and Applications*, (New York, NY, USA), pp. 57–62, Association for Computing Machinery, Jun. 2018.

[79] A. Alsharoa, H. Ghazzai, M. Yuksel, A. Kadri, and A. E. Kamal, "Trajectory optimization for multiple uavs acting as wireless relays," in *2018 IEEE International Conference on Communications Workshops, Kansas City, MO, USA*, pp. 1–6, Jul. 2018.

[80] O. S. Oubbati, A. Lakas, F. Zhou, M. Gne, N. Lagraa, and M. B. Yagoubi, "Intelligent uav-assisted routing protocol for urban vanets," *Comput. Commun.*, vol. 107, pp. 93—-111, Jul. 2017.

[81] M. Samir, C. Assi, S. Sharafeddine, D. Ebrahimi, and A. Ghrayeb, "Age of information aware trajectory planning of uavs in intelligent transportation systems: A deep learning approach," *IEEE Transactions on Vehicular Technology*, vol. 69, pp. 12382–12395, Sep. 2020.

[82] F. Nait-Abdesselam, A. Alsharoa, M. Y. Selim, D. Qiao, and A. E. Kamal, "Towards enabling unmanned aerial vehicles as a service for heterogeneous applications," *Journal of Communications and Networks*, vol. 23, pp. 212–221, Jun. 2021.

[83] X. Mu, Y. Liu, L. Guo, J. Lin, and H. V. Poor, "Intelligent reflecting surface enhanced multi-uav noma networks," *IEEE Journal on Selected Areas in Communications*, vol. 39, pp. 3051–3066, Jun. 2021.

[84] M. Mahbub and R. M. Shubair, "Intelligent reflecting surfaces in uav-assisted 6g networks: An approach for enhanced propagation and spectral characteristics," in *2022 IEEE International IOT, Electronics and Mechatronics Conference, Toronto, ON, Canada*, pp. 1–6, Jun. 2022.

[85] R. Liu, A. Liu, Z. Qu, and N. N. Xiong, "An uav-enabled intelligent connected transportation system with 6g communications for internet of vehicles," *IEEE Transactions on Intelligent Transportation Systems*, vol. 24, pp. 2045–2059, Feb. 2023.

[86] A. Traspadini, M. Giordani, and M. Zorzi, "Uav/hap-assisted vehicular edge computing in 6g: Where and what to offload?," in *2022 Joint European Conference on Networks and Communications & 6G Summit, Grenoble, France*, pp. 178–183, Jun. 2022.

[87] N. Rajatheva, I. Atzeni, S. Bicais, E. Bjornson, A. Bourdoux, S. Buzzi, C. D'Andrea, J.-B. Dore, S. Erkucuk, M. Fuentes, K. Guan, Y. Hu, X. Huang, J. Hulkkonen, J. M. Jornet, M. Katz, B. Makki, R. Nilsson, E. Panayirci, K. Rabie, N. Rajapaksha, M. Salehi, H. Sarieddeen, S. Shahabuddin, T. Svensson, O. Tervo, A. Tolli, Q. Wu, and W. Xu, "Scoring the terabit/s goal:broadband connectivity in 6g," Aug. 2020.

[88] B. Edwards and C. Hoffman, "What is 5g, and how fast is it?," Apr. 2022.

[89] C. de Looper and M. Jansen, "How fast is 5g? 5g speeds explained," Apr. 2022.

[90] Jamie, K. Schmid, K. Waters, L. Betzhold, B. Hadley, R. Mataosky, and J. Halleran, *Lidar 101: An Introduction to Lidar Technology, Data, and Applications*. National Oceanic and Atmospheric Administration Coastal Services Center, Nov. 2012.

[91] L. Wallace, A. Lucieer, C. Watson, and D. Turner, "Development of a uav-lidar system with application to forest inventory," *Remote Sensing*, vol. 4, pp. 1519–1543, Mar. 2012.

[92] R. A. Fowler, A. Samberg, M. J. Flood, and T. J. Greaves, "Topographic and terrestrial lidar," *Digital Elevation Model Technologies and Applications: The DEM Users Manual, 2nd edition. Bethesda, Maryland: American Society for Photogrammetry and Remote Sensing, 655p*, pp. 199–252, Jan. 2007.

[93] C. Wei and Z. Jian, "Application of intelligent uav onboard lidar measurement technology in topographic mapping," in *2021 IEEE International Conference on Emergency Science and Information Technology, Chongqing, China*, pp. 942–945, Nov. 2021.

[94] S. Sun and C. Salvaggio, "Aerial 3d building detection and modeling from airborne lidar point clouds," *IEEE Journal of Selected Topics in Applied Earth Observations and Remote Sensing*, vol. 6, pp. 1440–1449, May 2013.

[95] B. Anand, H. R. Kambhampaty, and P. Rajalakshmi, "A novel real-time lidar data streaming framework," *IEEE Sensors Journal*, vol. 22, pp. 23476–23485, Dec. 2022.

[96] Y. Hou, Z. Zhang, C. Wang, S. Cheng, and D. Ye, "Research on vehicle identification method and vehicle speed measurement method based on multi-rotor uav equipped with lidar," in *2020 3rd International Conference on Advanced Electronic Materials, Computers and Software Engineering, Shenzhen, China*, pp. 383–389, Apr. 2020.

[97] C. Chen, A. Jin, B. Yang, R. Ma, S. Sun, Z. Wang, Z. Zong, and F. Zhang, "Dcpld-net: A diffusion coupled convolution neural network for real-time power transmission lines detection from uav-borne lidar data," *International Journal of Applied Earth Observation and Geoinformation*, vol. 112, p. 102960, 2022.

[98] L. Diels, M. Vlaminck, B. De Wit, W. Philips, and H. Luong, "On the optimal mounting angle for a spinning lidar on a uav," *IEEE Sensors Journal*, vol. 22, no. 21, pp. 21240–21247, 2022.

[99] M. C. Lucic, H. Ghazzai, and Y. Massoud, "A generalized dynamic planning framework for green uav-assisted intelligent transportation system infrastructure," *IEEE Systems Journal*, vol. 14, pp. 4786–4797, Feb. 2020.

[100] H. Huang, A. V. Savkin, and C. Huang, "Decentralized autonomous navigation of a uav network for road traffic monitoring," *IEEE Transactions on Aerospace and Electronic Systems*, vol. 57, pp. 2558–2564, Aug. 2021.

[101] S. Shi, X. Wang, and H. Li, "Pointrcnn: 3d object proposal generation and detection from point cloud," in *2019 IEEE Conference on Computer Vision and Pattern Recognition*, pp. 770–779, Jun. 2019.

[102] Z. Osterwisch, A. Mauntel, and N. a. Nisbett, "Particulate matter detection in mines using 3d light detection and ranging technology," in *IEEE Wireless Communications and Networking Conference, Glasgow, Scotland, UK*, pp. 1–6, Mar. 2023.

[103] Z. Osterwisch, O. Rinchi, A. Alsharoa, H. Ghazzai, and Y. Massoud, "Multiple uav-lidar placement optimization under road priority and resolution requirements," in *IEEE International Conference on Communications, Rome, Italy*, pp. 1–6, May 2023.

VITA

Zachary Michael Osterwisch was born 26 years ago in St. Louis, Missouri. He was actively involved in sports and outdoor activities throughout his youth. In 2016, he completed high school at Francis Howell North in St. Charles, Missouri. Subsequently, his interest in video games and computers and his passion for understanding the world's workings led him to pursue an education in electrical engineering at Saint Louis University, where he remained for one semester before deciding to take time off from his studies. He resumed his education in the fall of 2018 at the Missouri University of Science and Technology (Missouri S&T).

During Zachary's time at Missouri S&T, he was a member of Tau Beta Pi, the National Society of Leadership and Success, and the Institute of Electrical and Electronics Engineers, and he served as president of the Backpacking Club. He discovered a more profound passion for computers during his undergraduate years and decided to join the Accelerated Bachelor of Science / Master of Science Program. This program allowed him to begin graduate coursework and research prematurely, later contributing to his graduate degree. Zachary graduated from Missouri S&T with Summa Cum Laude honors and earned his Bachelor of Science in electrical engineering in May 2022.

Zachary then continued his graduate research at Missouri S&T, where he simultaneously majored in computer engineering and remotely worked part-time for Sandia National Laboratories. His research focused on light detection and ranging technology, multirotor unmanned aerial vehicles, optimization, and computational intelligence, and he successfully published two papers on these topics [102, 103]. Zachary's hard work and determination secured him a full-time post-graduation research and development position at Sandia, where he will work as a rocket scientist. Zachary again graduated from Missouri S&T with honors in May 2023, earning his Master of Science in computer engineering before moving to Albuquerque, New Mexico.